

This is an Open Access document downloaded from ORCA, Cardiff University's institutional repository: <https://orca.cardiff.ac.uk/id/eprint/109765/>

This is the author's version of a work that was submitted to / accepted for publication.

Citation for final published version:

Hollstein, Martina, Mohtadi, Mahyar, Rosenthal, Yair, Moffa Sanchez, Paola, Oppo, Delia, Martínez Méndez, Gema, Steinke, Stephan and Hebbeln, Dierk 2017. Stable oxygen isotopes and Mg/Ca in planktic foraminifera from modern surface sediments of the Western Pacific Warm Pool: Implications for thermocline reconstructions. *Paleoceanography* 32 (11) , pp. 1174-1194. 10.1002/2017PA003122

Publishers page: <https://doi.org/10.1002/2017PA003122>

Please note:

Changes made as a result of publishing processes such as copy-editing, formatting and page numbers may not be reflected in this version. For the definitive version of this publication, please refer to the published source. You are advised to consult the publisher's version if you wish to cite this paper.

This version is being made available in accordance with publisher policies. See <http://orca.cf.ac.uk/policies.html> for usage policies. Copyright and moral rights for publications made available in ORCA are retained by the copyright holders.



1 **Stable oxygen isotopes and Mg/Ca in planktic foraminifera from modern surface**
2 **sediments of the Western Pacific Warm Pool: Implications for thermocline**
3 **reconstructions**

4
5 **Martina Hollstein^{1*}, Mahyar Mohtadi¹, Yair Rosenthal², Paola Moffa Sanchez³, Delia**
6 **Oppo⁴, Gema Martínez Méndez¹, Stephan Steinke⁵, Dierk Hebbeln¹**

7 ¹MARUM – Center for Marine Environmental Sciences, University of Bremen, Bremen,
8 Germany

9 ²Department of Marine and Coastal Sciences and Earth and Planetary Sciences, Rutgers, State
10 University of New Jersey, USA.

11 ³School of Earth and Ocean Sciences, Cardiff University, Cardiff, UK

12 ⁴Department of Geology and Geophysics, Woodshole Oceanographic Institution, Massachusetts,
13 USA

14 ⁵Department of Geological Oceanography, Xiamen University, Xiamen, China

15
16 *Corresponding author: Martina Hollstein (mhollstein@marum.de)

17
18 **Key Points:**

- 19 • Combined Mg/Ca and stable oxygen isotopes in planktic foraminifera tests from
20 accurately dated modern surface sediments
- 21 • Seawater oxygen isotope-salinity regressions for surface and subsurface waters in the
22 Western Pacific Warm Pool
- 23 • Calcification depth estimates and regional multispecies and species-specific Mg/Ca-
24 temperature calibrations
25

26 Abstract

27 Mg/Ca and stable oxygen isotope compositions ($\delta^{18}\text{O}$) of planktic foraminifera tests are
28 commonly used as proxies to reconstruct past ocean conditions including variations in the
29 vertical water column structure. Accurate proxy calibrations require thorough regional studies,
30 since parameters such as calcification depth and temperature of planktic foraminifera depend on
31 local environmental conditions. Here we present radiocarbon-dated, modern surface sediment
32 samples and water column data (temperature, salinity, seawater $\delta^{18}\text{O}$) from the Western Pacific
33 Warm Pool. Seawater $\delta^{18}\text{O}$ ($\delta^{18}\text{O}_{\text{SW}}$) and salinity are used to calculate individual regressions for
34 western Pacific surface and thermocline waters ($\delta^{18}\text{O}_{\text{SW}} = 0.37 \cdot S - 12.4$ and $\delta^{18}\text{O}_{\text{SW}} = 0.33 \cdot S -$
35 11.0). We combine shell $\delta^{18}\text{O}$ and Mg/Ca with water column data to estimate calcification depths
36 of several planktic foraminifera and establish regional Mg/Ca-temperature calibrations.

37 *Globigerinoides ruber*, *Globigerinoides elongatus* and *Globigerinoides sacculifer* reflect mixed
38 layer conditions. *Pulleniatina obliquiloculata* and *Neogloboquadrina dutertrei* and *Globorotalia*
39 *tumida* preserve upper and lower thermocline conditions, respectively. Our multispecies Mg/Ca-
40 temperature calibration ($\text{Mg/Ca} = 0.26 \exp(0.097 \cdot T)$) matches published regressions. Assuming
41 the same temperature sensitivity in all species, we propose species-specific calibrations that can
42 be used to reconstruct upper water column temperatures. The Mg/Ca-temperature dependencies
43 of *G. ruber*, *G. elongatus* and *G. tumida* are similar to published equations. However, our data
44 imply that calcification temperatures of *G. sacculifer*, *P. obliquiloculata* and *N. dutertrei* are
45 exceptionally warm in the western tropical Pacific, and thus, underestimated by previously
46 published calibrations. Regional Mg/Ca-temperature relations are best described by $\text{Mg/Ca} =$
47 $0.24 \exp(0.097 \cdot T)$ for *G. sacculifer* and by $\text{Mg/Ca} = 0.21 \exp(0.097 \cdot T)$ for *P. obliquiloculata* and *N.*
48 *dutertrei*.

49

50 1. Introduction

51 The Western Pacific Warm Pool (WPWP) is a major source of heat and water vapor to the global
52 atmosphere with far-reaching climate impacts [e.g. *Gagan et al.*, 2004]. The area is also thought
53 to play an essential role in the global overturning circulation, because it provides waters to the
54 Pacific equatorial current system and the Indonesian Throughflow, [e.g. *Gordon*, 1986]. Present
55 climate in the WPWP is mainly controlled by the Austral-Asian monsoon system and large-scale
56 climate phenomena such as the El Niño Southern Oscillation (ENSO). The regional climate is
57 strongly coupled to ocean conditions. Changes in the prevailing climate conditions affect, for
58 example, mixed layer depth and the thermocline structure [e.g. *DiNezio et al.*, 2011; *Vecchi et al.*,
59 2006]. Thus, reconstructing past hydrographic conditions and variations in the vertical structure of
60 the water column allow to draw conclusions on the regional WPWP climate evolution.

61

62 There is an ongoing debate how the thermocline depth varied throughout the past. For example,
63 some records indicate a thermocline deepening during the Last Glacial Maximum (LGM) [e.g.

64 *Bolliet et al.*, 2011], others indicate a thermocline shoaling during the same period [*Andreasen and*
65 *Ravelo*, 1997; *Beaufort et al.*, 2001; *de Garidel-Thoron et al.*, 2007; *Regoli et al.*, 2015; *Sagawa*
66 *et al.*, 2012] and yet others indicate no change compared to the modern ocean [*Patrick and Thunell*,
67 1997]. Many of these reconstructions are based on the calculation of differences between shell
68 Mg/Ca-derived temperature and/or $\delta^{18}\text{O}$ of planktic foraminifera calcifying at different depth
69 levels to estimate vertical temperature gradients within the upper water column [e.g. *Bolliet et al.*,
70 2011; *de Garidel-Thoron et al.*, 2007; *Regoli et al.*, 2015]. Previous studies used for example the
71 difference between shell Mg/Ca in *G. ruber* as surface indicator and *P. obliquiloculata* or *N.*
72 *dutertrei* as thermocline depth indicators [e.g. *Bolliet et al.*, 2011], or the difference between *G.*
73 *ruber sensu stricto* and *G. ruber sensu lato* (here referred to as *G. ruber* and *G. elongatus* following
74 *Aurahs et al.* [2011]) [*Regoli et al.*, 2015]. However, to choose species and interpret such proxy
75 records correctly, it is essential to understand how modern hydrographic conditions are reflected
76 in foraminiferal calcite.

77
78 The choice of species to use depends on regional calcification depths, which are determined by the
79 species preferences and local environmental conditions. However, although many paleoclimate
80 reconstructions for the WPWP exist, precise estimates of calcification depths are sparse in this
81 area. Published reconstructions rely on plankton tow and sediment trap studies in the central
82 equatorial Pacific, North Pacific or Indian Ocean [*Kawahata et al.*, 2002; *Kuroyanagi and*
83 *Kawahata*, 2004; *Mohtadi et al.*, 2011; *Peeters et al.*, 2002; *Rippert et al.*, 2016; *Watkins et al.*,
84 1996]. In addition, precise Mg/Ca-temperature calibrations are a prerequisite to convert Mg/Ca
85 into temperature. For the WPWP there are only two regional Mg/Ca-temperature calibrations [*Lea*
86 *et al.*, 2000; *Sagawa et al.*, 2012]. *Lea et al.* [2000] provide a species-specific calibration for *G.*
87 *ruber* and *Sagawa et al.* [2012] present a multispecies calibration. Both calibrations are exposed
88 to certain limitations. While the species-specific calibration might be biased by post-depositional
89 effects on the core top planktic foraminifera sample material [*Lea et al.*, 2000], the multispecies
90 equation of *Sagawa et al.* [2012] bases only on data from a single station. Besides, both calibrations
91 base on late Holocene sediments and therefore, might lack comparability to present hydrography.
92 Regional species-specific calibrations for subsurface planktic foraminifera species do not exist for
93 the WPWP. Subsequently, most proxy studies use Mg/Ca-temperature calibrations from other
94 areas [e.g. *Bolliet et al.*, 2011; *de Garidel-Thoron et al.*, 2007; *Regoli et al.*, 2015; *Tachikawa et*

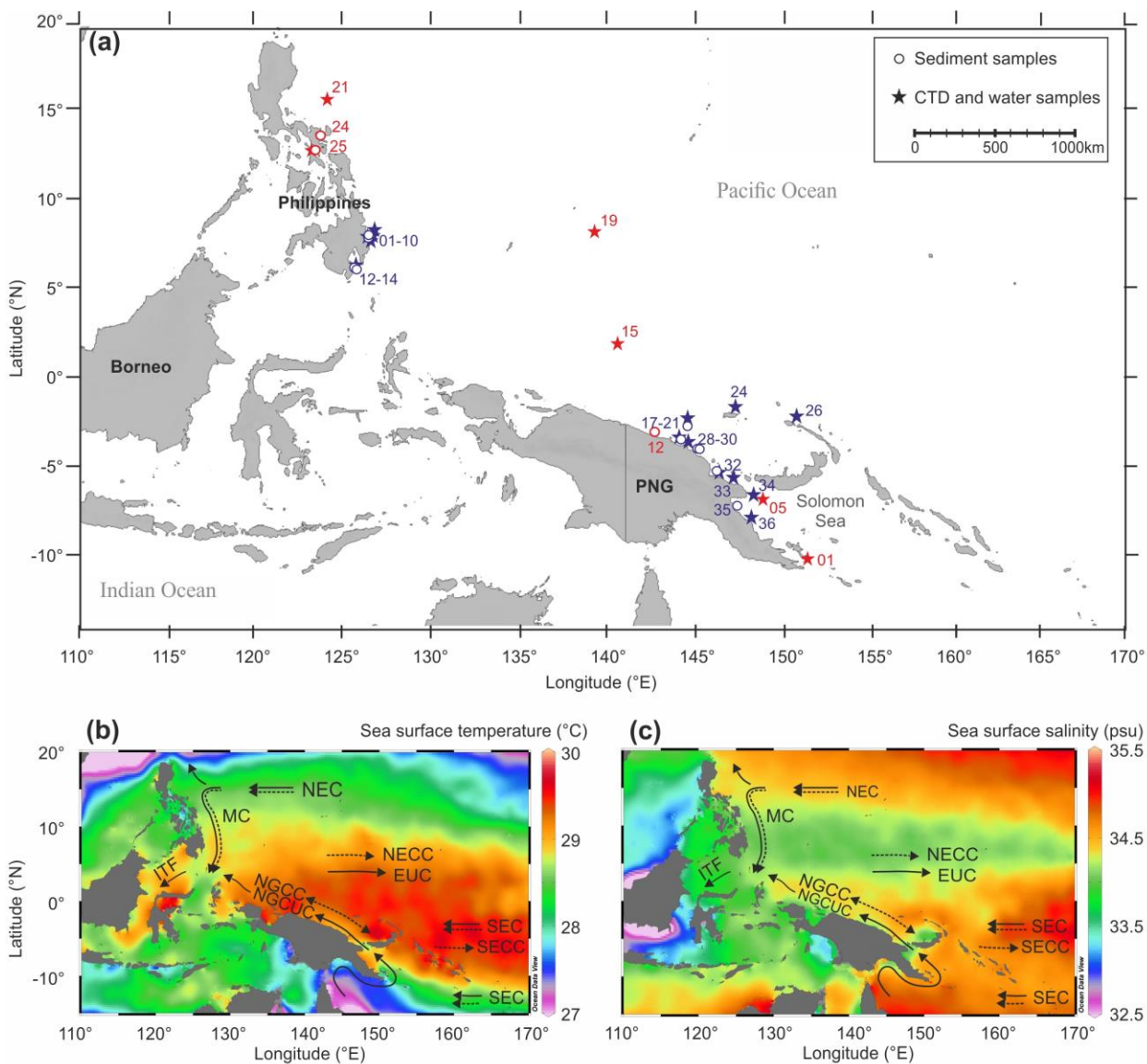
95 *al.*, 2014]. However, the adequacy of previously published Mg/Ca-temperature calibrations for the
96 WPWP has not yet been tested.

97
98 Here, we present paired Mg/Ca and $\delta^{18}\text{O}$ measurements on planktic foraminifera tests from
99 radiocarbon-dated, modern surface sediments in combination with water column data from stations
100 offshore the Philippines and Papua New Guinea (PNG) (Figure 1a and Table 1). Together, these
101 areas represent a major part of the WPWP. We estimate species-specific calcification depths and
102 temperatures of various planktic foraminifera species and establish regional Mg/Ca temperature
103 calibrations for the WPWP. In order to estimate calcification depths, we compare shell $\delta^{18}\text{O}$ with
104 depth profiles of expected equilibrium $\delta^{18}\text{O}$ of calcite ($\delta^{18}\text{O}_{\text{C}}$) at the respective locations. While
105 this is a common approach, an advantage of our study is the availability of concurrently measured
106 salinity and seawater $\delta^{18}\text{O}$ ($\delta^{18}\text{O}_{\text{SW}}$) data, upon which the calculated depth profiles of $\delta^{18}\text{O}_{\text{C}}$ are
107 based on. In this framework, we also calculate and provide regional $\delta^{18}\text{O}_{\text{SW}}$ -salinity regressions
108 for surface and subsurface water masses in the WPWP. Finally, we relate Mg/Ca to calcification
109 temperatures to find the most appropriate Mg/Ca calibration for each species and establish a
110 regional multispecies as well as monospecific Mg/Ca-temperature calibrations. We identify the
111 appropriate species to reconstruct past variations in mixed layer depth and thermocline structure
112 as well as the appropriate calibrations to convert Mg/Ca into temperature.

113
114 We note that the study is subject to certain limitations. First, it is based on surface sediments. This
115 bears the disadvantages that we do not have direct information about hydrographic parameters at
116 periods, when the calcite shells were built. Besides, we cannot fully exclude secondary influences
117 (e.g. dissolution) on our data and, we cannot resolve (intra-)seasonal changes in hydrography.
118 Second, our study includes water column data measured during two expeditions. These data
119 provide only snapshots of the WPWP hydrography. Moreover, we did not measure pH or $[\text{CO}_3^{2-}]$
120 and therefore, cannot fully exclude an effect of pH or $[\text{CO}_3^{2-}]$ on shell Mg/Ca, although it appears
121 negligible under ambient seawater conditions [Kırsakürek *et al.*, 2008; Russell *et al.*, 2004]. Third,
122 since the availability of modern sample material is a prerequisite for calibration studies, our sites
123 are exclusively located in the coastal WPWP, where sedimentation rates are higher than in the
124 open Pacific Ocean. The applicability of our calibrations for the open ocean WPWP needs to be
125 tested in future studies. Finally, especially species-specific calibrations are restricted by the fact,

126 that the temperature range within the study area is rather small. Where necessary, we discuss the
 127 limitations of the data in more detail (see section 5). Overall, the strengths of this study outweigh
 128 the mentioned limitations. Sediment-based studies have the great advantage that they are
 129 performed on the same material used for paleo studies. In relation to this, a great advantage of our
 130 study is the availability of (radiocarbon) dated, modern surface sediments. In addition, as
 131 mentioned above, our study greatly benefits from concurrent measurements of temperature,
 132 salinity and $\delta^{18}\text{O}_{\text{sw}}$.

133



134
 135 **Figure 1.** (a) Schematic map of the study area showing the stations, where water column data
 136 (stars) and surface sediments (dots) were collected during expeditions SO-228 (blue) and RR-1313

137 (red). Sites are labelled with station numbers. (b) Mean annual sea surface temperature and (c) sea
138 surface salinity derived from WOA13 [*Locarnini et al.*, 2013; *Zweng et al.*, 2013]. Temperature
139 and salinity maps were created with the Ocean data view software [*Schlitzer*, 2014]. Dashed and
140 solid arrows indicate main surface and (sub)surface currents influencing the study sites. MC –
141 Mindanao Current, NEC – North Equatorial Current, NECC – North Equatorial Counter Current,
142 EUC – Equatorial Undercurrent, NGCC – New Guinea Coastal Current, NGCUC – New Guinea
143 Coastal Undercurrent, SEC – South Equatorial Current, SECC – South Equatorial Countercurrent,
144 ITF – Indonesian Throughflow.
145

147 **Table 1.** Shell stable oxygen isotopes and Mg/Ca ratios of various planktic foraminifera species in surface sediments from the
 148 Western Pacific Ocean.

Core	Latitude (°N)	Longitude (°E)	Water depth (m)	<i>G. ruber</i> $\delta^{18}\text{O}$ (‰ VPDB)	<i>G. ruber</i> Mg/Ca (mmol/mol)	<i>G. elongatus</i> $\delta^{18}\text{O}$ (‰ VPDB)	<i>G. elongatus</i> Mg/Ca (mmol/mol)	<i>G. sacc.</i> $\delta^{18}\text{O}$ (‰ VPDB)	<i>G. sacc.</i> Mg/Ca (mmol/mol)	<i>P. obliq.</i> $\delta^{18}\text{O}$ (‰ VPDB)	<i>P. obliq.</i> Mg/Ca (mmol/mol)	<i>N.</i> <i>duertrei</i> $\delta^{18}\text{O}$ (‰ VPDB)	<i>N. duertrei</i> Mg/Ca (mmol/mol)	<i>G. tumida</i> (355-425 μm) $\delta^{18}\text{O}$ (‰ VPDB)	<i>G. tumida</i> (355-425 μm) Mg/Ca (mmol/mol)	<i>G. tumida</i> (>425 μm) $\delta^{18}\text{O}$ (‰ VPDB)	<i>G. tumida</i> (>425 μm) Mg/Ca (mmol/mol)
<i>Philippines</i>																	
RR1313-24 50MC	13.57	123.73	1055	-3.25 -3.15	5.28	-3.24	-	-2.78	3.81	-3.47	3.17	-1.84	-	-	-	-	-
RR1313-25 53MC	12.78	123.48	559	-2.95	5.30	-3.30	-	-	3.95	-	-	-	4.23	-	-	-	-
GeoB 17404-2	7.90	126.54	404	-3.03	5.47	-2.91	-	-2.69	3.95	-	-	-	-	-	-	-	-
GeoB 17410-3	7.87	126.59	771	-3.08	5.44 5.82	-3.79	5.46	-2.69 -2.89 -2.94 -2.55 -2.47	4.04	-	-	-	2.68	-	3.27	-	-
GeoB 17414-2	6.26	125.83	2188	-3.13	4.95	-3.01	-	-2.90	3.55	-2.34	2.69 2.74	-2.31 -2.23 -2.23 -2.12 -2.07	2.62	-	-	-	-
<i>Papua New Guinea</i>																	
GeoB 17419-2	-2.81	144.50	1887	-3.18 -3.14 -3.10 -3.15 -2.90	5.17 5.30	-3.05	5.37	-2.95	3.77	-2.15 -1.80 -1.69 -1.59 -1.57	2.27 2.51	-1.64	2.30	-0.70 -0.64 -0.16	1.79 1.89	-0.94	1.63
RR1313-12 30MC	-3.13	142.76	994	-3.74	5.30	-3.01	-	-3.39	4.26	-2.40	2.91	-	2.59	-	-	-	-
GeoB 17421-2	-3.55	144.20	588	-3.45	4.94	-3.43	5.42	-2.64	3.66	-2.20	2.70	-1.52 -1.42 -1.35 -1.27	1.95	-0.31	2.15	-	-
GeoB 17429-1	-4.10	145.20	1604	-3.02	5.13	-3.04 -2.81 -2.77 -2.73 -2.59	5.21	-2.62	3.74 3.85	-2.00	2.93	-2.01	2.24 2.39	-0.07	1.41	-0.08	1.72
GeoB 17430-2	-4.22	145.03	1160	-3.38 -3.31 -3.02 -2.98 -2.78	5.19	-2.98	5.14	-2.73	3.89 4.03	-2.15	2.80	-1.75	2.78	-0.01	1.43 1.76	-0.31	1.90
GeoB 17432-3	-5.34	146.20	1388	-3.24	5.30	-2.86	5.14 5.44	-2.62 -2.60 -2.60 -2.47 -1.72	3.58	-2.13	2.63	-2.09	1.54 3.09	-	1.35	0.06	1.56
GeoB 17435-2	-7.27	147.34	1001	-3.29	5.10 5.77	-3.24 -3.02 -2.89 -2.24	5.68	-2.81	3.88	-2.23	2.70 2.71	-2.09	2.26	-0.15	1.68	-0.45 -0.35 -0.08	1.43 1.85

149 **2. Study area**

150 The WPWP is characterized by exceptionally high ocean temperatures with sea surface
151 temperatures (SST) exceeding 28°C (Figure 1b) [Locarnini *et al.*, 2013]. Sea surface salinity
152 is about 34 psu (Figure 1c) [Zweng *et al.*, 2013]. The average mixed layer depth is about 50–
153 100 m [Locarnini *et al.*, 2013]. The upper thermocline waters are characterized by higher
154 salinities with maxima of around 34.5–35.0 psu off the Philippines and 35.5 psu off PNG.
155 Salinity maxima correspond to the North and South Pacific Tropical Waters (NPTW and
156 SPTW). The NPTW is formed within the western North Pacific Subtropical Gyre and
157 transported along the Philippines towards the equator by the Mindanao Current (MC) [Fine *et*
158 *al.*, 1994]. The SPTW originates in the South Pacific Suptropical Gyre [Tsuchiya *et al.*, 1989].
159 It is transported westwards by the SEC and along the coast of PNG by the New Guinea Coastal
160 Current (NGCC) and Undercurrent (NGCUC) system. Below the NPTW and SPTW waters are
161 characterized by lower salinities and are influenced by the Antarctic Intermediate Water
162 (AAIW) originating in the Southern Ocean and/or the North Pacific Intermediate water (NPIW)
163 with stronger predominance of AAIW offshore PNG and of NPIW offshore the Philippines
164 [Fine *et al.*, 1994; Zenk *et al.*, 2005].

165
166 The seasonal climate variability is mainly controlled by the Austral-Asian monsoon and leads
167 to only minor changes in the WPWP hydrography. Temperature and salinity variations are
168 smaller than 1-2°C and 1 psu [Locarnini *et al.*, 2013; Zweng *et al.*, 2013]. On interannual
169 timescales, El Niño Southern Oscillation (ENSO) affects surface ocean conditions as well as
170 the vertical structure of the water column in the WPWP with drier (wetter) conditions and a
171 shallower (deeper) thermocline during El Niño (La Niña) years.

172
173 Generally, the northern part of the study area is characterized by oligotrophic surface
174 conditions and a deep chlorophyll maximum (DCM) at the top of the thermocline [Radenac
175 *and Rodier*, 1996]. North of PNG nutrient concentrations and biological productivity are higher
176 than elsewhere in the WPWP [Radenac *et al.*, 2016]. However, the (vertical) distribution of
177 nutrients and chlorophyll is variable on (intra-)seasonal timescales [e.g. Higgins *et al.*, 2006;
178 Radenac *and Rodier*, 1996; Radenac *et al.*, 2016].

179
180 The (intra-)seasonal distribution of planktic foraminifera is controlled by different factors, such
181 as temperature, salinity and the availability of light and nutrients. Sediment trap data do not

182 reveal a clear picture of (intra-)seasonal preferences of planktic foraminifera in the study area
183 [*Kawahata et al.*, 2002; *Yamasaki et al.*, 2008]. Flux data from the equatorial Pacific showed
184 large (small) peaks during boreal summer (winter) under El Niño conditions and an increased
185 shell flux during the first half of the year under La Niña conditions [*Kawahata et al.*, 2002;
186 *Yamasaki et al.*, 2008]. Since no clear (intra-)seasonal pattern is indicated by these data we
187 assume that planktic foraminifera calcify perennially in the WPWP.

188

189 **3. Materials and methods**

190 3.1. Water column data and $\delta^{18}\text{O}_{\text{sw}}$ -salinity regressions

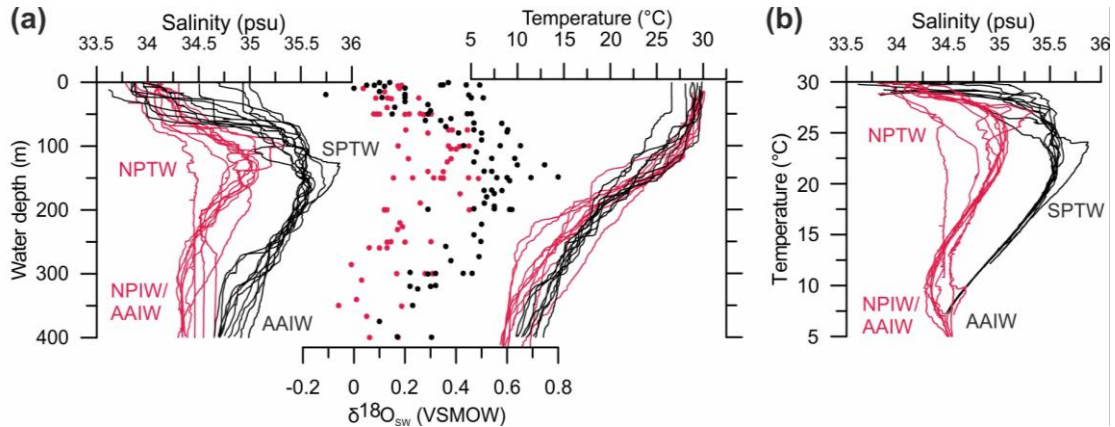
191 For this study, we used profiles of water column data, measured at fifteen stations offshore the
192 Philippines and PNG in May-June 2013 during RV SONNE expedition SO-228 [*Mohtadi et*
193 *al.*, 2013] and at six stations in August 2013 during RV REVELLE expedition RR-1313 (Figure
194 2) [*Rosenthal*, unpublished]. Temperature and salinity profiles are based on CTD
195 (Conductivity, Temperature and Depth) data. CTD data were measured using Seabird SBE911
196 (plus) CTD profilers during both expeditions. During CTD casts, water samples for stable
197 isotope analyses were collected from several water depths (supplementary information, Table
198 S1). Sampling was performed with CTD-sampling rosettes equipped with 24 Niskin bottles of
199 10–15 l volume. A part of the collected water was siphoned into 100 ml glass bottles for stable
200 isotope analyses, care was taken to avoid getting bubbles in the samples [*Mohtadi et al.*, 2013;
201 *Rosenthal*, unpublished]. All SO-228 samples (labelled as GeoB-samples in Table 1) were
202 sealed with wax and stored at 4°C before analysis. $\delta^{18}\text{O}_{\text{sw}}$ was determined with a Picarro
203 L1102-i CRDS water analyser with vaporization module V1102-i coupled to a CTC/Leaptec
204 PAL auto sampler at the Department of Geography and Earth Sciences, University of Erlangen-
205 Nuremberg. Calibration against Vienna Standard Mean Ocean Water (VSMOW) was achieved
206 by calibration to laboratory water standards calibrated against IAEA-standards VSMOW2 and
207 SLAP2 [*van Geldern and Barth*, 2012]. External reproducibility was 0.05 ‰. For the RR1313
208 samples, $\delta^{18}\text{O}_{\text{sw}}$ measurements were made at Rutgers University, New Jersey on a FISIONS
209 OPTIMA Mass Spectrometer equipped with a MicroMass Multiprep automatic sample
210 processing system after water sample equilibration with CO_2 using standard methods [*Epstein*
211 *and Mayeda*, 1953; *Fairbanks*, 1982]. All samples were run in duplicate. Precision was
212 estimated to be ± 0.03 ‰ (1 σ) as determined by multiple ($n = 12$) daily analyses of a laboratory
213 standard. Replicates must measure to within 0.068 ‰ to be included in the final data set.

214 Instrument linearity and accuracy was determined by comparison of the laboratory standard to
215 NBS standard water VSMOW, GISP, and SLAP. Accuracy was estimated to be within 0.03 ‰
216 by comparison of measurements of North Atlantic Bottom Water with VSMOW.

217

218 Generally, $\delta^{18}\text{O}_{\text{SW}}$ is linearly related to salinity [Craig and Gordon, 1965; Fairbanks et al.,
219 1992]. However, since both parameters are controlled by a number of factors, intercept and
220 slope of their relation are not the same for all ocean regions. Therefore, regional calibrations
221 are required [LeGrande and Schmidt, 2006]. Because the $\delta^{18}\text{O}_{\text{SW}}$ –salinity relation is not
222 constant over depth, we generated separate equations for surface and subsurface (SPTW and
223 NPTW) waters. For both, we investigated individual relations for the areas offshore the
224 Philippines and PNG as well as combined, more general, relations representing the entire study
225 area. We do not necessarily consider water samples from all stations and depth intervals.
226 Rather, for each equation we include samples that best characterize the relevant water masses
227 (supplementary information, Figure S1). The SPTW and NPTW regressions include only
228 samples that represent the core of these water masses, the WPWP wide subsurface regression
229 is more general and covers a slightly wider depth range.

230



231

232 **Figure 2.** (a) Salinity, $\delta^{18}\text{O}_{\text{SW}}$ and temperature profiles and (b) Temperature-salinity relations
233 at stations offshore the Philippines (red) and Papua New Guinea (black). Water masses are
234 labeled as follows: NPTW – North Pacific Tropical Water, SPTW – South Pacific Tropical
235 Water, NPIW – North Pacific Intermediate Water, AAIW – Antarctic Intermediate Water.

236

237 3.2. Sediment samples

238 Surface sediments were collected with multicorer devices during expedition SO-228 (nine
239 sampling sites) [Mohtadi et al., 2013] and during expedition RR-1313 (three sampling sites)

240 [Rosenthal *et al.*, unpublished]. The upper one or two cm of each multicore were washed over
241 63 μm sieves and dried.

242

243 All core sites are situated well above the present lysocline depth of 3300 m where carbonate
244 preservation is expected to be good [see Berger *et al.*, 1982 and references therein]. Presence
245 of aragonitic pteropod shells in most SO-228/GeoB core tops (including the core top from our
246 deepest site) further indicate a good carbonate preservation in our samples.

247

248 3.3. Dating

249 Age estimates of all GeoB sediment samples are based on accelerator mass spectrometry
250 (AMS) ^{14}C ages (Table 2). All ^{14}C ages were measured on monospecific *Globigerinoides*
251 *sacculifer* or on mixed *Globigerinoides ruber*, *G. elongatus* and *G. sacculifer* samples. The
252 measurements were carried out at the Keck Carbon Cycle Accelerator Mass Spectrometry
253 Laboratory, University of California, Irvine (UCI). Fraction modern carbon ($F^{14}\text{C}$) values
254 above one indicate modern ages for all ^{14}C dated samples (Table 2). In addition, a few GeoB
255 samples were treated with Rose Bengal and contained stained individuals, indicating that these
256 individuals died only very recently.

257

258 The RR-1313 samples did not contain enough foraminifera for radiocarbon dating. For age
259 control of these samples, we measured the carbon isotopic composition ($\delta^{13}\text{C}$) on about 10
260 specimens of *G. ruber* from the 250-300 μm size fraction from the upper 10 cm of each
261 multicore to check for the Suess effect (Figure S2). The Suess effect describes a rapid decrease
262 in seawater $\delta^{13}\text{C}$ going along with the depletion in ^{13}C of atmospheric CO_2 , which has been
263 caused by an increase in deforestation and burning of ^{12}C rich fossil fuels since the industrial
264 revolution [e.g. Böhm *et al.*, 1996; Friedli *et al.*, 1986]. The $\delta^{13}\text{C}$ measurements were
265 performed at Rutgers University, New Jersey using a Micromass Optima mass spectrometer,
266 coupled to an automatic line for carbonate preparation. The stable isotope values were
267 calibrated against the international Vienna Pee Dee Belemnite (VPDB) standard using an
268 internal standard, which is calibrated against the National Bureau of Standards (NBS) 19
269 standard. The long-term standard deviation for $\delta^{13}\text{C}$ was 0.06 ‰. Rapid drops in $\delta^{13}\text{C}$ from our
270 RR-1313 multicores are indicative for Suess effect and hence, modern ages of these surface
271 sediments (Figure S2). Thus, all samples used in this study reflect modern hydrographic
272 conditions of the WPWP.

273
274
275

Table 2. Radiocarbon dating of surface sediments from the Western Pacific Warm Pool. Results are expressed as fraction modern carbon ($F^{14}C$) and conventional ^{14}C ages.

Core	Lab-ID	Depth (cm)	Species	$F^{14}C$ \pm error	^{14}C age \pm error (years)	Cal. Age
GeoB 17404-2	142715	1-2	<i>G. ruber</i> , <i>G. elongatus</i> , <i>G. sacculifer</i>	1.042 ± 0.002	-325 ± 20	>1950 AD
GeoB 17410-3	158806	1-2	<i>G. ruber</i> , <i>G. elongatus</i> , <i>G. sacculifer</i>	1.064 ± 0.002	-490 ± 20	>1950 AD
GeoB 17414-2	158804	0-1	<i>G. ruber</i> , <i>G. elongatus</i> , <i>G. sacculifer</i>	1.058 ± 0.002	-445 ± 20	>1950 AD
GeoB 17419-2	142718	0-1	<i>G. sacculifer</i>	1.072 ± 0.002	-550 ± 20	>1950 AD
	142719	0-1	<i>G. sacculifer</i>	1.068 ± 0.003	-515 ± 20	>1950 AD
GeoB 17421-2	158805	0-1	<i>G. ruber</i> , <i>G. elongatus</i> , <i>G. sacculifer</i>	1.054 ± 0.002	-420 ± 15	>1950 AD
GeoB 17429-1	142725	0-1	<i>G. sacculifer</i>	1.054 ± 0.002	-415 ± 20	>1950 AD
GeoB 17430-2	142717	0-1	<i>G. ruber</i> , <i>G. elongatus</i> , <i>G. sacculifer</i>	1.058 ± 0.002	-445 ± 20	>1950 AD
GeoB 17432-3	142716	0-1	<i>G. sacculifer</i>	1.049 ± 0.002	-375 ± 20	>1950 AD
GeoB 17435-2	158803	0-1	<i>G. sacculifer</i>	1.066 ± 0.002	-500 ± 20	>1950 AD

276

277

3.4. Isotope and trace element analyses

278

279

280

281

282

283

284

285

286

287

288

289

290

291

292

Tests from the foraminiferal species *G. ruber*, *G. elongatus* and *G. sacculifer* (without sac-like final chamber) (all taken from the 250–355 μ m size fraction), *Neogloboquadrina dutertrei* and *Pulleniatina obliquiloculata* (355–425 μ m), and *Globorotalia tumida* (355–425 μ m and >425 μ m) were picked under a binocular for $\delta^{18}O$ and Mg/Ca analyses. For all species but *G. tumida*, specimens were separately picked for isotope and Mg/Ca analyses. *G. tumida* specimens were very rare in most of the samples. In order to ensure that fragments of several individuals were used for each measurement, 10 (where available) individuals were picked, crushed, homogenized and then separated for isotope and trace element analyses.

Around 40–120 μ g carbonate (around 3–10 specimens) were used for stable isotope analyses. The isotopic composition of all samples was measured at the MARUM-isotope laboratory, University of Bremen, Germany, using a Finnigan MAT 251 mass spectrometer, connected to an automatic line for carbonate preparation (type “Kiel III”). All isotope values were calibrated against the international Vienna Pee Dee Belemnite (VPDB) standard. The internal carbonate standard is a Solnhofen Limestone, which is calibrated to the NBS 19 standard. The analytical

293 standard deviation for $\delta^{18}\text{O}$ is below $\pm 0.07\%$. To check the reproducibility of the data we
294 performed up to four (depending on the available material) replicate measurements on 11
295 samples (Table 1). The results indicate an average standard deviation of 0.22% for $\delta^{18}\text{O}$.

296

297 For Mg/Ca analyses we used 30 (where available) well preserved specimens of *G. ruber* and
298 *G. elongatus*, 25 specimens of *G. sacculifer*, 15 specimens of *P. obliquiloculata* and *N.*
299 *dutertrei* and between 2 and 10 individuals of *G. tumida*. Although the presence of pteropods
300 indicates negligible effect of carbonate dissolution, all samples were weighed to estimate a
301 potential influence of dissolution on the Mg/Ca records. Samples were gently crushed between
302 two glass plates to open the chambers. The full trace metal cleaning procedure followed the
303 protocol described by *Barker et al.* [2003] with an additional reductive step [*Boyle and*
304 *Keigwin*, 1985; *Rosenthal et al.*, 1997; *Rosenthal et al.*, 1999]. Samples were dissolved in
305 0.0065 M HNO_3 , centrifuged for 10 min at 10000 rpm and diluted with 0.5 N HNO_3 . The final
306 calcium concentration of the samples was on average 3.2 mM . Trace metal ratios were
307 measured at Rutgers University, New Jersey with a Thermo Fisher/Finnigan Element XR
308 sector-field inductively coupled plasma mass spectrometer (ICP-MS). Mg/Ca measurements
309 were performed in low resolution ($\Delta m/m = 300$). Measured ratios were blank corrected. Mass
310 drift and matrix effects and the long term precision of the data were controlled with in house
311 standard solutions [*Rosenthal et al.*, 1999]. All Mg/Ca values are given in mmol/mol. Replicate
312 measurements on 14 samples revealed an average standard deviation of 0.23 mmol/mol (Table
313 1). To monitor the cleaning efficacy Al/Ca, Fe/Ca and Mn/Ca were measured alongside Mg/Ca.
314 None of these ratios showed a covariance with Mg/Ca (Figure S3). Mg/Ca ratios of individual
315 species do not show a correlation to water depth or shell normalized weights (Figure S4). Thus,
316 we exclude any substantial effect of carbonate dissolution on shell Mg/Ca values.

317

318 3.5. Estimation of calcification depths and temperatures

319 In order to estimate species-specific calcification depths we compare shell $\delta^{18}\text{O}$ of individual
320 species with depth-profiles of $\delta^{18}\text{O}_C$, assuming that all species calcified in isotopic equilibrium
321 with seawater. The water depth where shell $\delta^{18}\text{O}$ matches the expected $\delta^{18}\text{O}_C$ is considered to
322 reflect the calcification depth of the respective species at the site.

323 Depth-profiles of expected $\delta^{18}\text{O}_C$ were calculated from SO-228 and RR-1313 CTD salinity
324 profiles as follows. First, $\delta^{18}\text{O}_{\text{SW}}$ was calculated from salinity using here established regional
325 (WPWP) $\delta^{18}\text{O}_{\text{SW}}$ -salinity equations (equations I and II in section 4.1). The average uncertainty

326 in the calculated $\delta^{18}\text{O}_{\text{SW}}$ given as the average standard deviation between measured and
327 calculated $\delta^{18}\text{O}_{\text{SW}}$ is 0.05 ‰. It was necessary to calculate $\delta^{18}\text{O}_{\text{SW}}$ from CTD salinity instead
328 of using the measured $\delta^{18}\text{O}_{\text{SW}}$ to obtain continuous profiles. Results were converted from
329 VSMOW to the VPDB scale by subtracting 0.27 ‰ [Hut, 1987]. Then, we applied a set of
330 commonly used $\delta^{18}\text{O}$ -temperature equations (Table 3) to predict equilibrium $\delta^{18}\text{O}_{\text{C}}$ using CTD
331 temperature and the previously calculated $\delta^{18}\text{O}_{\text{SW}}$. Finally, we matched shell $\delta^{18}\text{O}$ to the $\delta^{18}\text{O}_{\text{C}}$
332 profiles. Since surface sediments were not always taken at the same positions as CTD, we
333 matched shell $\delta^{18}\text{O}$ to profile(s) from those station(s), which are nearest to the core sites. To
334 determine uncertainties of the calcification depth of each species and core site we estimated
335 the calcification depths based on shell $\delta^{18}\text{O}$ with added/subtracted species-specific standard
336 deviations. Depending on the standard deviation and the shape of the profiles, average
337 uncertainties range between ± 10 and 30 m.
338 CTD temperatures at depths corresponding to the estimated calcification depths give an
339 estimate of the calcification temperatures for each species and core site. For *G. elongatus*, *P.*
340 *obliquiloculata* and *N. dutertrei* only a few samples from the Philippines contained enough
341 individuals to perform isotope analyses. For *G. tumida* none of the Philippines' samples
342 contained enough specimens and therefore, depth and temperature estimates for this species
343 are only representative for the area offshore PNG.

344
345 **Table 3.** General and species-specific $\delta^{18}\text{O}$ -temperature equations used in this study

Reference	Species	Linear equations		
		$T (^{\circ}\text{C}) = a - b (\delta^{18}\text{O}_{\text{C}} - \delta^{18}\text{O}_{\text{SW}})$		
		a	b	
<i>Bemis et al.</i> [1998]	<i>O. universa (HL)</i>	14.9	-4.8	
<i>Bouvier-Soumacnac and Duplessy</i> [1985]	<i>N. dutertrei</i>	10.5	-6.58	
<i>Farmer et al.</i> [2007]	<i>G. ruber</i>	15.4	-4.78	
	<i>G. sacculifer</i>	16.2	-4.94	
	<i>N. dutertrei</i>	14.6	-5.09	
	<i>P. obliquiloculata</i>	16.8	-5.22	
<i>Mulitza et al.</i> [2003]	<i>G. tumida</i>	13.1	-4.95	
	<i>G. ruber</i>	14.2	-4.44	
	<i>G. sacculifer</i>	14.91	-4.35	
<i>Shackleton</i> [1974]	<i>Uvigerina sp.</i>	16.9	-4.0	
<i>Spero et al.</i> [2003]	<i>G. sacculifer</i>	12.0	-5.67	
		Quadratic equations		
		$T (^{\circ}\text{C}) = a - b (\delta^{18}\text{O}_{\text{C}} - \delta^{18}\text{O}_{\text{SW}}) + c (\delta^{18}\text{O}_{\text{C}} - \delta^{18}\text{O}_{\text{SW}})^2$		
		a	b	c
<i>Kim and O'Neil</i> [1997]	inorganic	16.1	-4.64	0.09

347 **4. Results**

348 4.1. Water column data and $\delta^{18}\text{O}_{\text{SW}}$ -salinity regressions

349 The $\delta^{18}\text{O}_{\text{SW}}$ -salinity relations for the study area during summer 2013 reveal that a $\delta^{18}\text{O}_{\text{SW}}$
350 increase of about 0.3 to 0.4 ‰ corresponds to a salinity increase of 1 psu (Figure 3).
351 Regressions for surface waters offshore the Philippines and PNG (considering only samples
352 from the Bismarck and Solomon Seas) are very similar (Figure 3a, blue and red dots,
353 respectively). The regression line for surface waters offshore PNG shows only a slightly steeper
354 slope and consequently, a smaller intercept. Taking all SO-228 and RR-1313 stations across
355 the WPWP into account (Figure 3a, all black and colored dots) the surface $\delta^{18}\text{O}_{\text{SW}}$ -salinity
356 relation can be described as:

357

358
$$\delta^{18}\text{O}_{\text{SW}} = 0.37 (\pm 0.03) * S - 12.4 (\pm 1.0) \quad (R^2 = 0.80) \quad (\text{I})$$

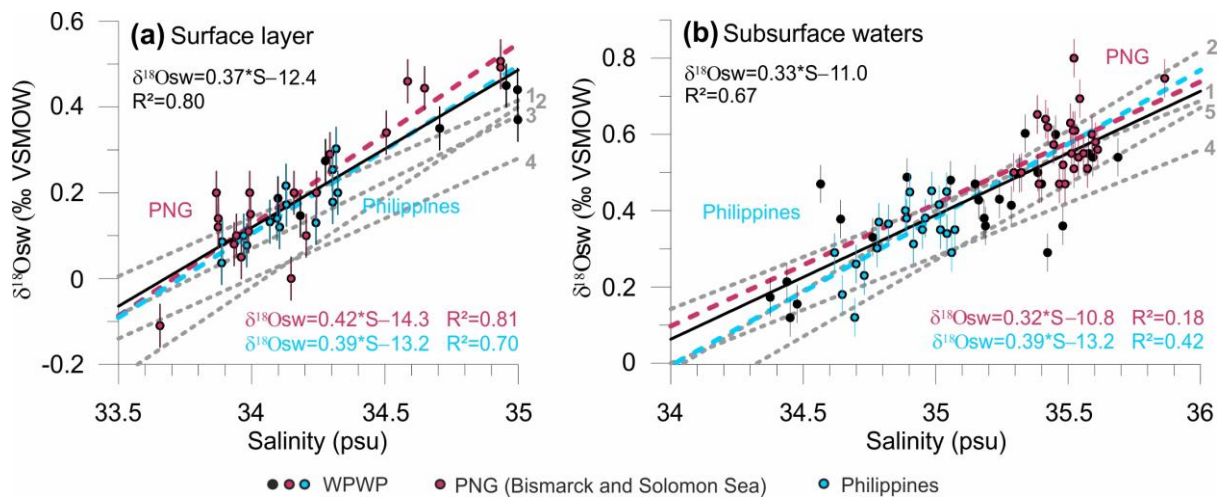
359

360 Regression lines describing the $\delta^{18}\text{O}_{\text{SW}}$ -salinity relations for subsurface waters (NPTW and
361 SPTW) show a shallower slope than for surface waters with slightly higher intercepts (Figure
362 3b). Due to the very small salinity ranges within the NPTW and SPTW it is difficult to assess
363 a robust relationship for each of these water masses. The regressions also greatly depend on
364 the depths and number of stations included in each equation. However, although NPTW and
365 SPTW have different characteristics (see Figure 2), their $\delta^{18}\text{O}_{\text{SW}}$ -salinity regressions are very
366 similar to each other. Therefore, we also provide one equation for WPWP subsurface waters
367 that includes all SO-228 and RR-1313 sample stations (Figure 3b, all black and colored dots).

368

369
$$\delta^{18}\text{O}_{\text{SW}} = 0.33 (\pm 0.03) * S - 11.0 (\pm 1.1) \quad (R^2 = 0.67) \quad (\text{II})$$

370



371

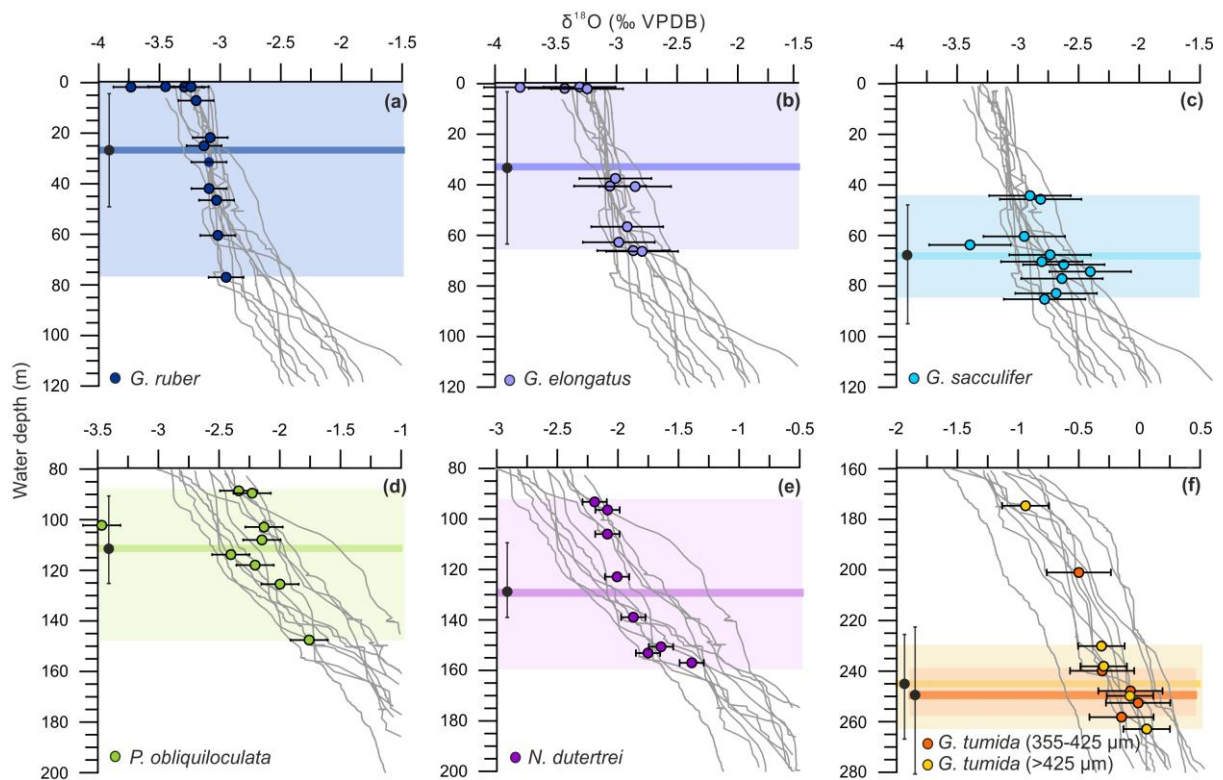
372 **Figure 3.** Regional $\delta^{18}\text{O}_{\text{sw}}$ –salinity relations for (a) surface and (b) subsurface waters in the
 373 Western Pacific Warm Pool. Dots indicate individual samples included in the regressions. Red
 374 and blue colors indicate subsets of samples included in the regional regressions off Papua New
 375 Guinea (PNG) and the Philippines, respectively. Black dots indicate samples from sites that
 376 are not included in the regional regressions. Black lines indicate regression lines for the entire
 377 study area and colored lines for the subareas. Gray stippled lines show regional $\delta^{18}\text{O}_{\text{sw}}$ –salinity
 378 equations published by 1. *Fairbanks et al.* [1997], 2. *Morimoto* [2002], 3/5. *Leech et al.* [2013],
 379 4. [*LeGrande and Schmidt*, 2011]. Bars indicate laboratory standard deviations for oxygen
 380 isotope measurements.

381

382 4.2. Calcification depth

383 In general, shell $\delta^{18}\text{O}$ increases with increasing calcification depth of the species. *G. ruber* and
 384 *G. elongatus* record the lowest $\delta^{18}\text{O}$ values and *G. tumida* records the highest $\delta^{18}\text{O}$ values. *G.*
 385 *sacculifer*, *P. obliquiloculata* and *N. dutertrei* calcify in between. Shell $\delta^{18}\text{O}$ and our derived
 386 mean calcification depths of the species used are very similar offshore the Philippines and
 387 PNG. Therefore, in our discussion we do not distinguish between samples from the Philippines
 388 and PNG. Figure 4 and Table 4 give $\delta^{18}\text{O}$ -derived depths for all species as estimated by
 389 applying the $\delta^{18}\text{O}$ -temperature equation of *Bemis et al.* [1998]. Depth estimates for each species
 390 applying different $\delta^{18}\text{O}$ -temperature equations in comparison are provided in the
 391 supplementary information (Figures S4–6).

392



393

394 **Figure 4.** Shell $\delta^{18}\text{O}$ derived calcification depth estimates for several planktic foraminifera
 395 (colored dots) in the Western Pacific Warm Pool. Gray lines indicate depth profiles of predicted
 396 $\delta^{18}\text{O}_c$ calculated from individual CTD casts (see section 3.5 for details). The average
 397 calcification depth at each core site is determined by matching shell $\delta^{18}\text{O}$ to $\delta^{18}\text{O}_c$ of the
 398 profile(s) nearest to the respective core site. Horizontal bars indicate species-specific standard
 399 deviations for shell $\delta^{18}\text{O}$, vertical bars on black dots show exemplarily average uncertainties in
 400 calcification depth derived by projecting shell $\delta^{18}\text{O}$ with added/subtracted standard deviations
 401 on the $\delta^{18}\text{O}_c$ profiles. The uncertainty of the $\delta^{18}\text{O}_c$ profiles arising from the average standard
 402 deviation between measured and calculated $\delta^{18}\text{O}_{sw}$ is 0.05 ‰ (not shown). Colored shading
 403 indicates calcification depth ranges for the individual species in the study area. The average
 404 calcification depth is highlighted by colored horizontal bars. Note the different scaling of the
 405 axes in different panels. Individual data points, which are shown outside the range of predicted
 406 $\delta^{18}\text{O}_c$ do not match any profile (see text).

407 **Table 4.** Calcification depth and temperatures. The calcification depth of each species and core site was estimated by comparing shell
 408 $\delta^{18}\text{O}$ to depth profiles of predicted $\delta^{18}\text{O}$ calcite. Predicted $\delta^{18}\text{O}_\text{C}$ was calculated from CTD salinity applying the $\delta^{18}\text{O}_\text{sw}$ -salinity equations
 409 of this study and the $\delta^{18}\text{O}$ -temperature equation of *Bemis et al.* [1998] using CTD temperature. We assigned a depth of 0 m to samples
 410 that did not match any profile. Calcification temperatures are CTD temperatures at depth corresponding to the estimated calcification
 411 depths.

412

Core	<i>G. ruber</i> (250-355 μm)		<i>G. elongatus</i> (250-355 μm)		<i>G. sacculifer</i> (250-355 μm)		<i>P. obliquiloculata</i> (355-425 μm)		<i>N. dutertrei</i> (355-425 μm)		<i>G. tumida</i> (355-425 μm)		<i>G. tumida</i> (>425 μm)		
	Depth (m)	Temp. ($^{\circ}\text{C}$)	Depth (m)	Temp. ($^{\circ}\text{C}$)	Depth (m)	Temp. ($^{\circ}\text{C}$)	Depth (m)	Temp. ($^{\circ}\text{C}$)	Depth (m)	Temp. ($^{\circ}\text{C}$)	Depth (m)	Temp. ($^{\circ}\text{C}$)	Depth (m)	Temp. ($^{\circ}\text{C}$)	
<i>Philippines</i>															
RR1313-24 50MC	7	29.8	0	29.6	85	28.4	0	29.8	140	24.3	-	-	-	-	
RR1313-25 53MC	77	28.3	0	28.8	-	-	-	-	-	-	-	-	-	-	
GeoB 17404-2	47	28.9	57	28.5	83	27.8	-	-	-	-	-	-	-	-	
GeoB 17410-3	22	29.3	0	29.9	70	28.2	-	-	-	-	-	-	-	-	
GeoB 17414-2	25	29.2	37	28.7	45	28.2	88	25.8	94	25.3	-	-	-	-	
<i>Papua New Guinea</i>															
GeoB 17419-2	32	29.7	40	29.8	60	29.6	147	24.6	150	24.2	200	18.8	175	20.9	
RR1313-12 30MC	0	29.7	-	-	0	29.7	114	27.5	-	-	-	-	-	-	
GeoB 17421-2	0	29.7	0	29.7	77	28.3	117	26.7	157	23.1	240	17.7	-	-	
GeoB 17429-1	60	29.0	67	28.6	72	27.9	125	25.8	123	25.8	248	16.4	250	15.9	
GeoB 17430-2	42	29.2	63	28.7	68	28.5	108	26.3	153	24.7	252	15.8	230	17.6	
GeoB 17432-3	0	29.4	66	28.6	75	27.5	103	26.2	107	26.0	-	-	263	15.6	
GeoB 17435-2	0	28.9	40	28.9	45	26.7	90	26.9	97	26.2	258	16.6	238	17.7	

413

414

415 4.2.1. Mixed layer species: *G. ruber*, *G. elongatus* and *G. sacculifer*

416 Average shell $\delta^{18}\text{O}$ values are very similar for *G. ruber* and *G. elongatus* (-3.19 and -3.11 ‰,
417 Table 1). This implies very similar calcification depths for both species in the WPWP.
418 Depending on the selected $\delta^{18}\text{O}$ -temperature equation, shell $\delta^{18}\text{O}$ derived mean calcification
419 depths range from 0 to 45–105 m (Figures 4 and S4). Applying the $\delta^{18}\text{O}$ -temperature equations
420 of *Bemis et al.* [1998] and *Shackleton* [1974] the estimated depth range is within the upper 80
421 m of the water column for both, *G. ruber* and *G. elongatus*. By applying the equations of *Kim*
422 *and O'Neil* [1997] and *Farmer et al.* [2007] calcification depths shoal to 0–45 m and 0–65 m,
423 respectively, while the application of the species-specific equation of *Mulitza et al.* [2003]
424 result in a slightly deeper depth range (0–105 m) (Figure S5a).

425
426 Shell $\delta^{18}\text{O}$ of *G. sacculifer* varies around -2.73 ‰ (excluding RR1313-12 30MC) (Table 1).
427 Applying different $\delta^{18}\text{O}$ -temperature equations, the mean calcification depth varies between 45
428 and 95 m. It ranges from 45 to 85 m using the equation of *Bemis et al.* [1998] (Figure 4c) and
429 from 55 to 95 m applying the $\delta^{18}\text{O}$ -temperature equations of *Shackleton* [1974] and *Spero et*
430 *al.* [2003]. The equations of *Farmer et al.* [2007] and *Kim and O'Neil* [1997] lead to slightly
431 shallower calcification depths (0–70 m) and the equation of *Mulitza et al.* [2003] to deeper
432 calcification depths (70–110 m) (Figure S5b). Note that sample RR1313-12 30MC shows an
433 extremely low $\delta^{18}\text{O}$ value (-3.39 ‰), which does not match any profile.

434

435 4.2.2. Upper thermocline species: *P. obliquiloculata* and *N. dutertrei*

436 Shell $\delta^{18}\text{O}$ of *P. obliquiloculata* varies around -2.15 ‰ (excluding RR1313-24 50MC) (Table
437 1). For the majority of the samples this indicates a calcification depth between 90 and 125 m
438 when applying the $\delta^{18}\text{O}$ -temperature equation of *Bemis et al.* [1998] (Figure 4d). Applying the
439 equations of *Shackleton* [1974] or *Bouvier-Soumagnac and Duplessy* [1985] leads to very
440 similar calcification depths (85–120 and 90–130 m), the equations of *Kim and O'Neil* [1997]
441 and *Farmer et al.* [2007] leads to slightly shallower calcification depths (70-105 and 40-75 m)
442 (Figure S6a). Our foraminifera tests from site GeoB 17419-2 record exceptionally high $\delta^{18}\text{O}$
443 values resulting in, compared to the other core sites, relatively deeper (20–40 m) calcification
444 depths. With a $\delta^{18}\text{O}$ value of -3.47 ‰ (Table 1), sample RR1313-24 50MC does not match any
445 $\delta^{18}\text{O}_\text{C}$ profile.

446

447 The *N. dutertrei* average shell $\delta^{18}\text{O}$ of -1.88 ‰ is slightly higher than that of *P. obliquiloculata*.
448 By using the equations of *Bemis et al.* [1998], *Shackleton* [1974] or *Farmer et al.* [2007] shell
449 derived calcification depths vary between around 90 and 160 m (Figures 4e and S5b). The
450 application of the $\delta^{18}\text{O}$ -temperature equation from *Kim and O'Neil* [1997] or *Bouvier-*
451 *Soumagnac and Duplessy* [1985] result in slightly shallower or deeper depth ranges (80–150
452 or 95–155 m) (Figure S6b).

453

454 4.2.3. Lower thermocline species: *G. tumida*

455 Average shell $\delta^{18}\text{O}$ of *G. tumida* is -0.15 ‰ for the 355–425 μm size fraction and -0.14 ‰ for
456 the >425 μm size fraction (excluding GeoB 17419-2) (Table 1). Shell $\delta^{18}\text{O}$ of individual
457 samples differ by maximal 0.3 ‰. Hence, under the restriction of the small set of samples, our
458 data indicate, that there is no major size effect on the calcification depths of *G. tumida*. Based
459 on the equation of *Bemis et al.* [1998] the calcification depth of *G. tumida* at most sites is
460 between 230 and 265 m water depth (Figure 4f). The application of the equations from
461 *Shackleton* [1974] and *Kim and O'Neil* [1997] results in slightly shallower calcification depths,
462 ranging between 195 and 235 m. Based on the species-specific equation of *Farmer et al.* [2007]
463 the estimated calcification depths are slightly deeper, ranging between 255 and 310 m (Figure
464 S7). Exceptionally low $\delta^{18}\text{O}$ in *G. tumida* shells from GeoB 17419-2 indicates up to 70 m
465 shallower calcification depth at this site, independent of the size fraction used.

466

467 4.3. Shell Mg/Ca

468 Mg/Ca ratios recorded in the Philippines and PNG samples are very similar. *G. ruber* and *G.*
469 *elongatus* record highest Mg/Ca, averaging 5.26 and 5.37 mmol/mol, respectively. Shell
470 Mg/Ca in *G. sacculifer* varies around 3.85 mmol/mol. *N. dutertrei* and *P. obliquiloculata* show
471 similar shell Mg/Ca varying around 2.60 and 2.66 mmol/mol, respectively. *G. tumida* shows
472 lowest Mg/Ca ratios around 1.88 mmol/mol (355–425 μm) and 1.69 mmol/mol (>425 μm).
473 Hence, average Mg/Ca of the different species confirms the results obtained from oxygen
474 isotope ratios with calcification depths being shallowest for *G. ruber*, *G. elongatus* and *G.*
475 *sacculifer*, intermediate for *P. obliquiloculata* and *N. dutertrei* and deepest for *G. tumida*.
476 Mg/Ca ratios of *P. obliquiloculata* in RR1313-24 50MC, *N. dutertrei* in RR1313-53MC, and
477 *G. tumida* in GeoB 17410-3 are exceptionally high (3.17 mmol/mol, 4.23 mmol/mol, and 3.27
478 mmol/mol) (Table 1). The high Mg/Ca value of *P. obliquiloculata* in RR1313-24 50MC goes

479 along with exceptionally low $\delta^{18}\text{O}$ and could therefore indicate an extremely shallow
480 calcification depth at this site. Due to the limited number of specimens of *N. dutertrei* in
481 RR1313-25 53MC and *G. tumida* in GeoB 17410-3, we could not measure the oxygen isotope
482 composition in these samples.
483

484 **5. Discussion**

485 5.1. Water column data and $\delta^{18}\text{O}_{\text{SW}}$ -salinity regressions

486 Generally, our surface and subsurface $\delta^{18}\text{O}_{\text{SW}}$ -salinity regressions are within the range of
487 published WPWP regressions [Fairbanks *et al.*, 1997; Leech *et al.*, 2013; LeGrande and
488 Schmidt, 2011; Morimoto, 2002]. However, slope and/or intercept differ from previous
489 regression lines. Especially the regressions of Fairbanks *et al.* [1997], LeGrande and Schmidt
490 [2011] and the surface regression of Leech *et al.* [2011] show shallower slopes (around 0.3)
491 and accordingly, larger intercepts (between -10.47 and -9.14) than our regressions. The
492 regression of Morimoto *et al.* [2002] is almost identical to our PNG surface equation ($\delta^{18}\text{O}_{\text{SW}}$
493 = $0.42 \cdot \text{S} - 14.3$). Since $\delta^{18}\text{O}_{\text{SW}}$ -salinity relations depend on local environmental conditions,
494 deviations are most probably due to different sampling sites, water depths and periods.
495

496 For the first time, we generated equations for individual water masses (surface waters, NPTW
497 and SPTW). Our results reveal that for both, WPWP wide and regional regressions, the ratio
498 between $\delta^{18}\text{O}_{\text{SW}}$ and salinity is higher in surface than in subsurface waters. Therefore, it appears
499 reasonable to use different $\delta^{18}\text{O}_{\text{SW}}$ -salinity regressions for surface and subsurface water masses.
500 The regression coefficients of our regression lines (Figure 3) indicate that the application of a
501 more general, WPWP wide regression for combined NPTW and SPTW is more robust than
502 individual regressions for the NPTW and SPTW. This is due to the very small salinity range
503 within the NPTW offshore the Philippines and the SPTW offshore PNG.
504

505 5.2. Calcification depths and temperatures

506 Accurate calcification depth estimates are indispensable to deduce precise calcification
507 temperatures for each species. The accuracy of the depth estimates depends on the precision of
508 the $\delta^{18}\text{O}_{\text{SW}}$ -salinity equation applied, the choice of the $\delta^{18}\text{O}$ -temperature equation, the
509 availability of local water column data, the seasonal and interannual variations in local

510 hydrography and possible shell disequilibrium effects [see *Regenberg et al.*, 2009; *Steph et al.*,
511 2009].

512

513 A comparison between predicted $\delta^{18}\text{O}_C$ calculated using discrete $\delta^{18}\text{O}_{\text{SW}}$ measured in water
514 samples and predicted $\delta^{18}\text{O}_C$ using $\delta^{18}\text{O}_{\text{SW}}$ calculated from CTD salinity shows that the
515 calculated values reproduce measured $\delta^{18}\text{O}$ precisely (Figure S8). The average deviation
516 between calculated and measured $\delta^{18}\text{O}_{\text{SW}}$ is ± 0.07 ‰, the maximal deviation is ± 0.35 ‰ and
517 only 6 out of 98 samples yielded $\delta^{18}\text{O}_{\text{SW}}$ differences larger than 0.20 ‰ (see Table S2). The
518 comparison provides reliability to the accuracy of the $\delta^{18}\text{O}_{\text{SW}}$ -salinity equations for our
519 sampling period and sites.

520

521 For the following analyses we use calcification depth estimates based on the $\delta^{18}\text{O}$ -temperature
522 equation that was generated by *Bemis et al.* [1998] in a culture experiment for *O. universa*.
523 Although it has been obtained on a single species not used in our study, this equation is
524 commonly used for other planktic foraminiferal species [e.g. *Mohtadi et al.*, 2014; *Spero et al.*,
525 2003; *Thunell et al.*, 1999] and its application gives realistic results for all species used here.
526 The equations of *Shackleton* [1974], *Bouvier-Soumagnac and Duplessy* [1985], and *Spero et*
527 *al.* [2003] lead to similar calcification depths. The quadratic equation of *Kim and O'Neil* [1997]
528 results in marginally shallower depths for surface and similar depths for subsurface dwellers.
529 The application of the equations of *Farmer et al.* [2007] result in slightly shallower
530 calcification depths. The equations of *Farmer et al.* [2007] are based on sample material from
531 much greater water depths (mostly 3000-4000 m) where carbonate is affected by dissolution
532 [*Hertzberg and Schmidt*, 2013] which would increase $\delta^{18}\text{O}$ in foraminiferal tests.
533 Consequently, the application of these equations would underestimate calcification depths. The
534 equations proposed by *Mulitza et al.* [2003] result in deeper calcification depths. These
535 equations are based on plankton tow studies and might overestimate calcification depths due
536 to lower $\delta^{18}\text{O}$ in shells of living foraminifera [see *Regenberg et al.*, 2009 and references
537 therein].

538

539 Based on the assumption that planktic foraminifera calcify perennially in the WPWP we
540 assume that our $\delta^{18}\text{O}$ data represent mean annual conditions. However, we note that data from
541 individual samples might be biased and reflect other than normal conditions (e.g. a single
542 season or El Niño/La Niña conditions). We are well aware that our hydrographic data show a
543 snapshot and therefore, do not necessarily represent mean annual hydrography. However,

544 seasonal temperature and salinity variations are very small in our study area and mostly
545 restricted to the mixed layer (see section 2). Interannual variations in ocean hydrography are
546 mainly caused by ENSO variability. Our water column data were collected during a normal
547 year and are thus, not biased to El Niño or La Niña conditions. Considering the paucity of
548 continuous subsurface temperature, salinity and especially $\delta^{18}\text{O}_{\text{SW}}$ data from the WPWP, our
549 work provides the first simultaneous measurements on these parameters at different water
550 depths at stations in close proximity to our core sites and thus, the hitherto most suitable
551 hydrographic estimates for the determination of calcification depths and temperatures.

552

553 Nonetheless, we also compared shell $\delta^{18}\text{O}$ with depth-profiles of $\delta^{18}\text{O}_{\text{C}}$ calculated by using
554 mean annual temperature and salinity data from the World Ocean Atlas 13 (WOA13)
555 [Locarnini *et al.*, 2013; Zweng *et al.*, 2013]. Shell $\delta^{18}\text{O}$ of most *G. ruber* and *G. elongatus*
556 samples do not match the WOA13 $\delta^{18}\text{O}_{\text{C}}$ profiles. WOA13 derived calcification depths of *G.*
557 *sacculifer* extent over a larger depth range than SO-228 and RR-1313 CTD (from here on
558 referred to as CTD) calcification depths. WOA13 depth estimates of *P. obliquiloculata*, *N.*
559 *dutertrei* and *G. tumida* differ only slightly from CTD derived depth estimates (maximal 35 m)
560 with a tendency to shallower depths. Overall, for our study, the application of CTD data gives
561 more realistic results than the application of WOA13 data.

562

563 Previous studies have shown that many species do not calcify in isotopic equilibrium with
564 seawater [see Ravelo and Hillaire-Marcel, 2007 and references therein]. Potential reasons are
565 the photosynthetic activity of symbionts, incorporation of low $\delta^{18}\text{O}$ metabolic CO_2 , species-
566 specific calcification rates, the addition of gametogenic calcite, and possibly carbonate ion
567 concentrations of the ambient seawater [see Ravelo and Hillaire-Marcel, 2007 and references
568 therein]. Disequilibrium effects depend on local conditions and the sample material used. For
569 most species used in our study, negative disequilibrium effects ranging between 0.0 and 1.0 ‰
570 are presumed [see Lončarić *et al.*, 2006; Niebler *et al.*, 1999 and references therein]. No vital
571 effects are reported for *G. tumida*. Correcting for negative disequilibrium effects would
572 increase shell $\delta^{18}\text{O}$, and subsequently result in deeper calcification depths and colder
573 calcification temperatures [see discussion in Regenberg *et al.*, 2009]. However, the large
574 variety of factors that could possibly influence shell $\delta^{18}\text{O}$ makes it difficult to correct $\delta^{18}\text{O}$ for
575 disequilibrium effects precisely. In addition, most published $\delta^{18}\text{O}$ -temperature equations do not
576 take into account biological disequilibrium effects on $\delta^{18}\text{O}$. Therefore, we did not correct $\delta^{18}\text{O}$
577 values for disequilibrium effects.

578

579 Overall, our results show that *G. ruber* and *G. elongatus* calcify within the mixed layer (0–80
580 m) and *G. sacculifer* calcifies at the bottom of the mixed layer (45–85 m). *P. obliquiloculata*
581 and *N. dutertrei* calcify within the upper thermocline, whereby our $\delta^{18}\text{O}$ values indicate that *N.*
582 *dutertrei* calcifies within a larger depth range (90–160 m) than *P. obliquiloculata* does (90–125
583 m). *G. tumida* seems to calcify well below *P. obliquiloculata* and *N. dutertrei* within the lower
584 thermocline at depth between 230 and 265 m. In relation to water masses, this means that *G.*
585 *ruber*, *G. elongatus* and *G. sacculifer* calcify in surface waters. *P. obliquiloculata*, and *N.*
586 *dutertrei* calcify predominantly within the NPTW offshore the Philippines and within the
587 SPTW offshore PNG. *G. tumida* calcifies within the transition between NPTW/SPTW and
588 NPIW or AAIW. Our depth estimates generally agree with results from sediment traps and
589 plankton tows in the central equatorial Pacific, North Pacific and Indian Oceans [*Kuroyanagi*
590 *and Kawahata*, 2004; *Mohtadi et al.*, 2009; *Peeters et al.*, 2002; *Rippert et al.*, 2016; *Watkins*
591 *et al.*, 1996]. However, our data show a tendency to somewhat deeper absolute calcification
592 depths and wider depth ranges for most species, probably owing to a generally thick mixed
593 layer and deep thermocline in the WPWP. Recent results from the eastern WPWP indicate even
594 deeper habitat depths of planktic foraminifera [*Rippert et al.*, 2016]. Such differences in
595 absolute calcification depths are likely related to the specific regional hydrographic conditions
596 in each study area. For *G. ruber* and *G. elongatus*, our data imply very similar calcification
597 depths. This is in sharp contrast to studies from the South China Sea and North Pacific Ocean
598 that suggest a deeper habitat depth for *G. elongatus* [*Kawahata*, 2005; *Steinke et al.*, 2005;
599 *Wang*, 2000] but in agreement with studies from the eastern Indian Ocean and the Caribbean
600 Sea, which suggest the same habitat depth for both species [*Mohtadi et al.*, 2009; *Thirumalai*
601 *et al.*, 2014].

602

603 5.3. Mg/Ca versus calcification temperatures

604 A large number of studies revealed that Mg/Ca in planktic foraminiferal tests show an
605 exponential relationship with ocean temperatures [e.g. *Anand et al.*, 2003; *Cléroux et al.*, 2008;
606 *Dekens et al.*, 2002; *Elderfield and Ganssen*, 2000; *McConnell and Thunell*, 2005; *Mohtadi et*
607 *al.*, 2009; *Mohtadi et al.*, 2011; *Nürnberg et al.*, 1996; *Regenberg et al.*, 2009]. Some culture
608 and core top studies also described a positive salinity effect on shell Mg/Ca of planktic
609 foraminifera [*Arbuszewski et al.*, 2010; *Ferguson et al.*, 2008; *Kırsakürek et al.*, 2008; *Mathien-*
610 *Blard and Bassinot*, 2009; *Nürnberg et al.*, 1996]. However, studies suggesting a significant

611 salinity influence have been criticized due to substantial dissolution effects, seasonality
612 [Arbuszewski *et al.*, 2010] or diagenetic alteration [Ferguson *et al.*, 2008] on the sample
613 material [Hertzberg and Schmidt, 2013; Hönisch *et al.*, 2013]. However, in our study area the
614 salinity range is rather small (between 33.9 and 35.6 psu). Variations between stations at water
615 depths that correspond to the calcification depth of individual foraminifera species at the
616 corresponding core sites are below 1.2 psu. There is no significant correlation between Mg/Ca
617 and salinity (R-values range between 0.00 and 0.35 for individual species). Besides, shell
618 Mg/Ca in samples from offshore the Philippines and PNG are very similar, although these areas
619 are influenced by water masses characterized by different salinities (Figure 2). Therefore, we
620 argue that shell Mg/Ca in our samples is not biased by salinity. Some studies also indicate a
621 negative effect of pH or [CO₃²⁻] on Mg/Ca [Evans *et al.*, 2016; Kısakürek *et al.*, 2008; Lea *et al.*
622 *et al.*, 1999; Russell *et al.*, 2004; Spero *et al.*, 2015]. To date, it is not clear whether pH or [CO₃²⁻
623] exert a dominant control on Mg/Ca [Allen *et al.*, 2016; Evans *et al.*, 2016]. Moreover, the
624 effect is neither constant over temperature [Spero *et al.*, 2015], nor the same for different
625 planktic foraminifera species [e.g. Allen *et al.*, 2016] and some studies provide confidence that
626 the effect is negligible for ambient seawater conditions [Kısakürek *et al.*, 2008; Russell *et al.*,
627 2004]. Since pH or [CO₃²⁻] were not measured during both SO-228 and RR-1313 expeditions,
628 we cannot estimate the range of these parameters over the study area. We do not apply any
629 corrections for possible effects of carbonate chemistry on shell Mg/Ca, while we cannot fully
630 exclude such effect on our samples. More extensive culture and/or sediment trap studies are
631 required to quantify the effect pH or [CO₃²⁻] on Mg/Ca of the various planktic foraminifera
632 species.

633

634 Mg/Ca to temperature calibrations are usually expressed as $Mg/Ca = B \exp(A * Temperature)$.
635 We combined data of all species and compared shell Mg/Ca to CTD temperature at $\delta^{18}O$ -
636 derived calcification depths in a multispecies approach (Figure 5). A depth of 0 m was assigned
637 to samples, where shell $\delta^{18}O$ did not match the $\delta^{18}O_C$. Mg/Ca and temperature show a clear
638 exponential relationship (Figure 5). Previous studies suggest that this relationship is best
639 described by a reduced major axis (or geometric mean) regression (RMA) of the natural Log
640 of (Mg/Ca) against calcification temperature [Anand *et al.*, 2003; Rosenthal and Lohmann,
641 2002]. An advantage of the RMA is that it accounts for both, uncertainties in Mg/Ca and
642 calcification temperatures. Especially in field studies, calcification temperatures inherit an
643 intrinsic scatter that arises from a range of different factors including uncertainties in the depth
644 estimates or seasonality for example.

645 Using the RMA approach, the multispecies Mg/Ca-temperature relation is described by the
646 following equation:

647

$$648 \quad \text{Mg/Ca} = 0.26 (\pm 0.04) \exp 0.097 * T (\pm 0.006) \quad (\text{III})$$

649

650 The calculation followed *Isobe et al.* [1990]. The uncertainties of the slope and intercept are
651 given as standard deviations assuming that the intrinsic scatter of the data dominates any errors
652 of the measurement process.

653

654 For comparison, we also calibrated shell Mg/Ca against WOA13 mean annual temperatures.
655 Despite the differences in estimated calcification depths, WOA13 derived calcification
656 temperatures are very similar to CTD derived calcification temperatures. The reason is that
657 temperatures of the WOA13 climatology are generally lower than our CTD temperatures at the
658 same depth levels. Due to the similarity of the calcification temperatures, the WOA13 derived
659 regression is within the error range of the regression based on CTD derived calcification
660 temperatures. (A = 0.101, B = 0.24).

661

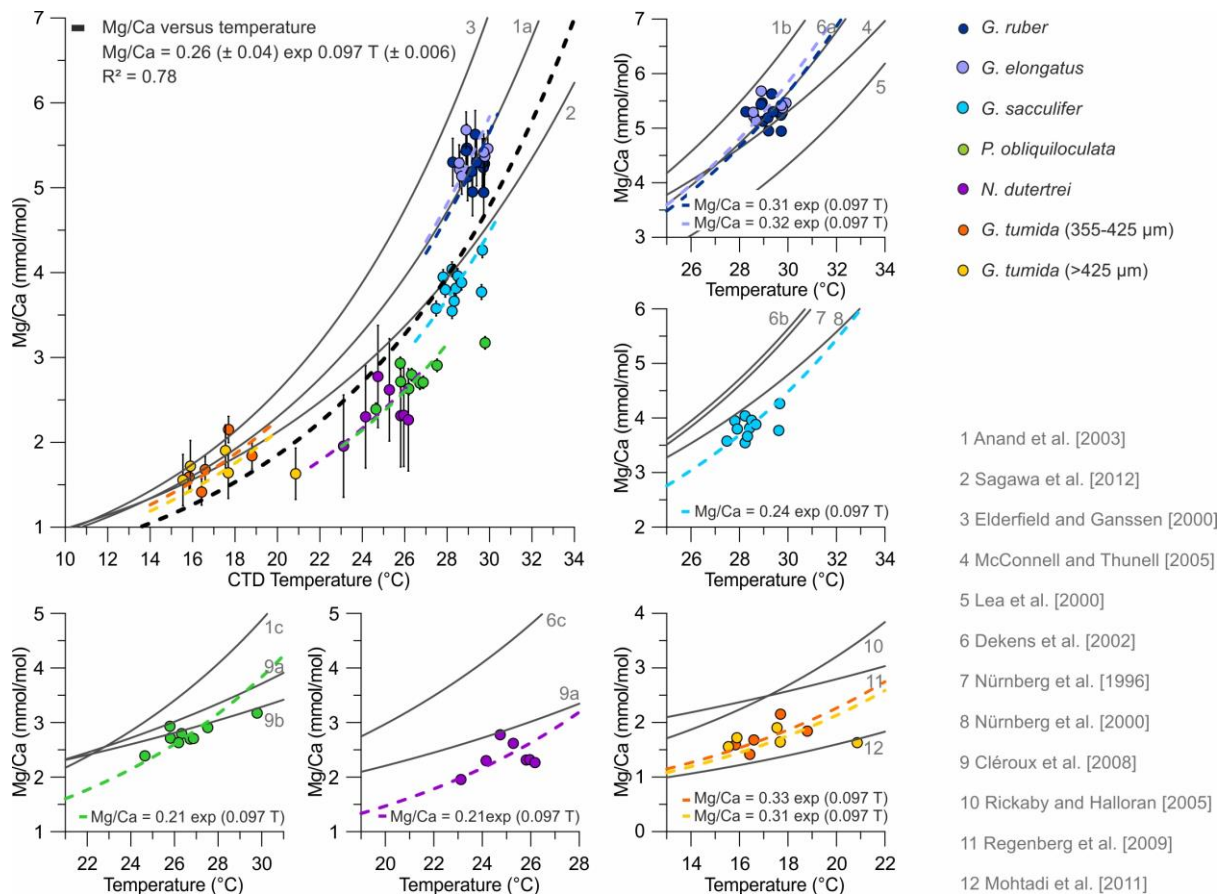
662 Our multispecies Mg/Ca-temperature relation is in good agreement with previously published
663 multispecies and species-specific temperature calibrations (Figure 5 and Table 5). However,
664 comparing our calibration to published ones, it has to be noted that our calibration is based on
665 samples that were treated by reductive cleaning, whereas most published calibrations are based
666 on samples cleaned without a reductive step. Previous studies indicate that the reductive
667 cleaning leads to a decrease in Mg/Ca [e.g. *Barker et al.*, 2003; *Xu et al.*, 2010]. To estimate
668 the effects on the Mg/Ca-temperature relations, we applied a correction assuming that the
669 Mg/Ca relations were reduced by about 10 % in all samples [e.g. *Barker et al.*, 2003; *Martin*
670 *and Lea*, 2002; *Rosenthal et al.*, 2004]. We note that some studies suggest different values for
671 individual species [e.g. *Xu et al.*, 2010], but since exact rates of Mg/Ca loss are unknown for
672 most species, we presume a constant rate of 10 % for all species. The resulting regression line
673 shows the same slope as the original calibration (0.097), and an only slightly modified intercept
674 (0.24). Thus, the modified calibration is within the error range of the original one.

675

676 A multispecies equation does not seem accurate enough to describe the Mg/Ca-temperature
677 relation of individual species in the WPWP. For example, all the *G. ruber* and *G. elongatus*
678 samples fall above, and all the *P. obliquiloculata* and *N. dutertrei* samples fall below the

679 regression line. That means, calcification temperatures of *G. ruber* and *G. elongatus* are
680 overestimated, and those of *P. obliquiloculata* and *N. dutertrei* are underestimated by the
681 multispecies regression. For that reason, species-specific regression lines are additionally
682 required to reconstruct calcification temperatures for individual species precisely. Since the
683 temperature range between the sites in our study area is very narrow, it is difficult to determine
684 the temperature sensitivity for individual species unequivocally. Hence, we calculated regional
685 species-specific regressions by assuming the same temperature sensitivity, $A = 0.097$, as it was
686 calculated by the multispecies approach, for all species (Figure 5). The resulting regression
687 lines for *G. ruber* and *G. elongatus* are very similar to the multispecies and species-specific
688 regression published by *Anand et al.* [2003] or *Dekens et al.* [2002], respectively ($Mg/Ca =$
689 $0.39 \exp 0.09 * T$). For the temperature range relevant for this study the regression lines of *G.*
690 *tumida* fall next to the multispecies regression lines of *Anand et al.* [2003] and *Sagawa et al.*
691 [2012]. However, especially slope and intercept of the *Sagawa et al.* [2012] regression differ
692 from those of our species-specific regression (Table 5) and it is important to note that the slope
693 affects the amplitude of temperature variations in paleorecords. The regression lines of *G.*
694 *sacculifer*, *P. obliquiloculata* and *N. dutertrei* deviate from previously published correlations
695 (Figure 5). Calcification temperatures of these species are exceptionally warm in the western
696 tropical Pacific Ocean despite deeper calcification depths and thus, *G. sacculifer*, *P.*
697 *obliquiloculata* and *N. dutertrei* require regional, species-specific Mg/Ca-temperature
698 calibrations. Assuming the temperature sensitivity calculated by the multispecies approach (A
699 $= 0.097$) our data indicate an intercept of $B = 0.24$ for *G. sacculifer* and an intercept of $B =$
700 0.21 for both *P. obliquiloculata* and *N. dutertrei* (Figure 5).

701



702

703 **Figure 5.** Shell Mg/Ca versus calcification temperature for different planktic foraminifera
 704 species. Black bars indicate species-specific standard deviations of Mg/Ca. Black and colored
 705 dashed lines indicate regional multispecies and species-specific regressions calculated with a
 706 RMA regression (this study). Gray solid lines show published multispecies (large graph) and
 707 species-specific (small graphs) regression lines. Numbers denote published calibrations (see
 708 also table 5). Note that a, b and c refer to different calibrations in the same publication.

709

710

711 **Table 5.** Multispecies and species-specific Mg/Ca temperature in comparison to previously
 712 published relations. Calibration numbers introduced in figure 5 are given in gray.

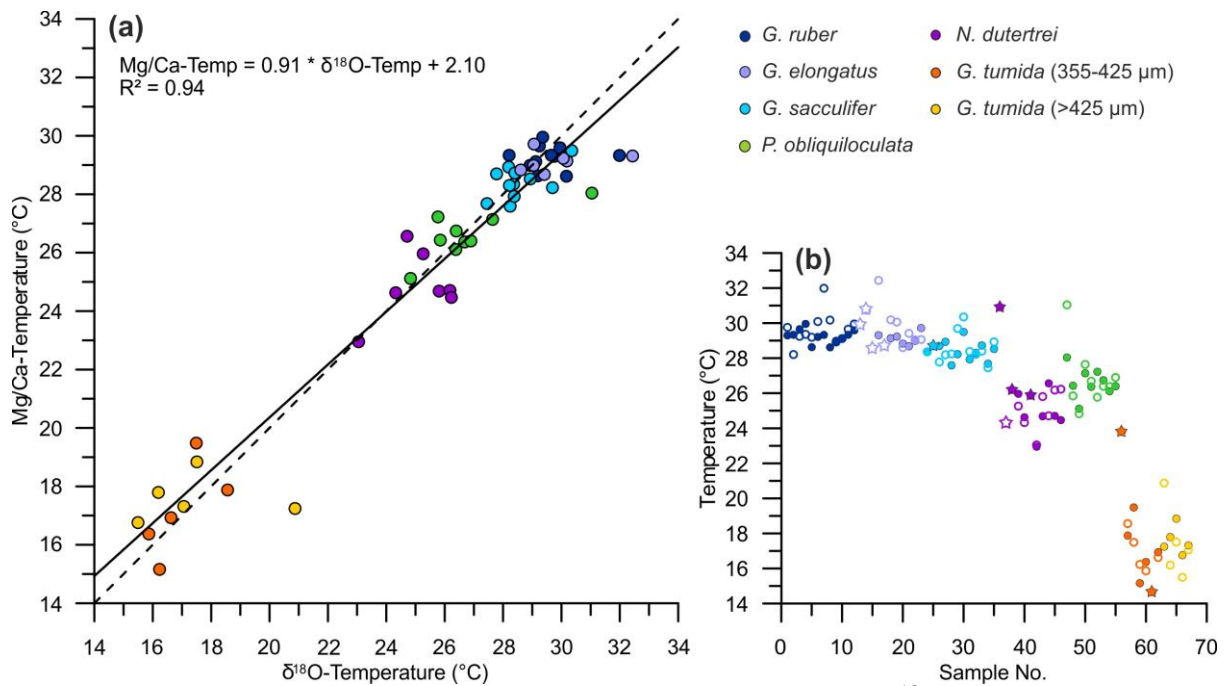
Reference	Species	Exponential relation Mg/Ca = B exp (A*Temperature)	
		A	B
<i>Anand et al.</i> [2003] (1a)	multispecies	0.09	0.38
<i>Sagawa et al.</i> [2011] (2)	multispecies	0.077	0.455
<i>Elderfield and Ganssen</i> [2000] (3)	multispecies	0.1	0.352
This study	multispecies	0.097	0.26
<i>Anand et al.</i> [2003] (1b)	<i>G. ruber</i>	0.09	0.44
<i>McConnell and Thunell</i> [2005] (4)	<i>G. ruber</i>	0.068	0.69

<i>Lea et al.</i> [2000] (5)	<i>G. ruber</i>	0.089	0.3
<i>Dekens et al.</i> [2002] (6a)	<i>G. ruber</i>	0.09	0.38
This study	<i>G. ruber</i>	0.097	0.31
This study	<i>G. elongatus</i>	0.097	0.32
<i>Dekens et al.</i> [2002] (6b)	<i>G. sacculifer</i>	0.09	0.37
<i>Nürnberg et al.</i> [1996] (7)	<i>G. sacculifer</i>	0.089	0.39
<i>Nürnberg et al.</i> [2000] (8)	<i>G. sacculifer</i>	0.076	0.49
This study	<i>G. sacculifer</i>	0.097	0.24
<i>Anand et al.</i> [2003] (1c)	<i>P. obliquiloculata</i>	0.09	0.328
<i>Cléroux et al.</i> [2008] (9b)	<i>P. obliquiloculata</i>	0.039	1.02
This study	<i>P. obliquiloculata</i>	0.097	0.21
<i>Dekens et al.</i> [2002] (6c)	<i>N. dutertrei</i>	0.08	0.6
This study	<i>N. dutertrei</i>	0.097	0.21
<i>Cléroux et al.</i> [2008] (9a)	Deep dwelling species	0.052	0.78
<i>Rickaby and Halloran</i> [2005] (10)	<i>G. tumida</i>	0.09	0.53
<i>Regenberg et al.</i> [2009] (11)	<i>G. tumida</i>	0.041	1.23
<i>Mohtadi et al.</i> [2011] (12)	<i>G. tumida</i>	0.068	0.41
This study	<i>G. tumida</i> (355-425 μm)	0.097	0.33
This study	<i>G. tumida</i> (>425 μm)	0.097	0.31

713

714 A comparison of Mg/Ca-temperatures and calcification temperatures gives a measure of the
715 uncertainty inherent in the Mg/Ca-temperature calibrations [*Anand et al.*, 2003]. We compared
716 Mg/Ca-temperatures calculated by the application of species-specific calibrations to $\delta^{18}\text{O}$ -
717 derived calcification temperatures (Figure 6). The average standard error between Mg/Ca and
718 $\delta^{18}\text{O}$ -derived calcification temperatures is 0.5°C. The consistency of Mg/Ca and $\delta^{18}\text{O}$ -derived
719 calcification temperatures validates our previous steps and assumptions, and gives further
720 evidence, that Mg/Ca and $\delta^{18}\text{O}$ data are not influenced by secondary effects.

721



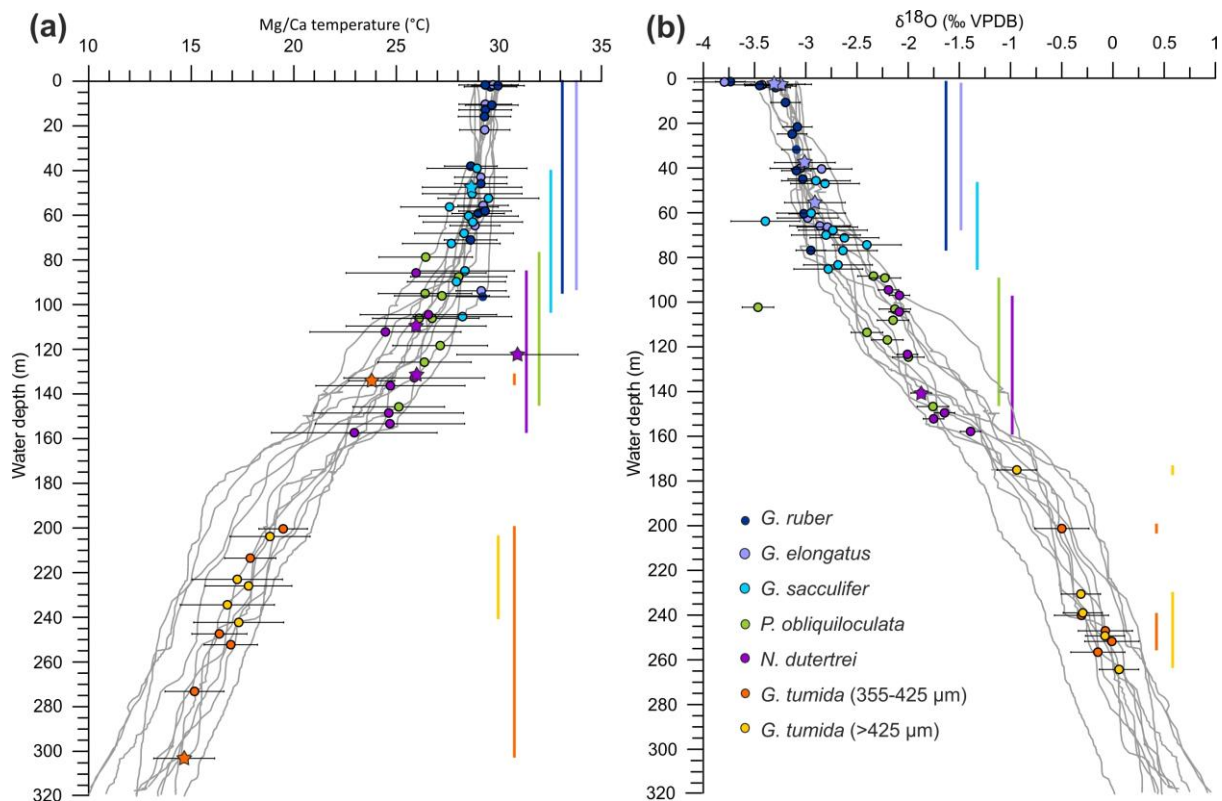
722 **Figure 6.** Consistency of temperature estimates. (a) Mg/Ca- versus δ¹⁸O-derived calcification
 723 temperatures. Mg/Ca-temperatures are based on species-specific regressions; δ¹⁸O-
 724 temperatures were calculated with the equation of *Bemis et al.* [1998]. The black solid line
 725 shows the correlation between Mg/Ca- and δ¹⁸O-temperatures. For comparison, the 1:1
 726 relationship is shown (stippled line). (b) Comparison of Mg/Ca-temperatures (filled symbols)
 727 and δ¹⁸O-temperatures (open symbols). Note that (a) includes only samples with paired δ¹⁸O
 728 and Mg/Ca measurements, whereas (b) includes all samples where δ¹⁸O or Mg/Ca
 729 measurements are available. Samples where only δ¹⁸O or Mg/Ca measurements are available
 730 are marked with stars. Sample numbers are related to cores as defined in Table S3.
 731
 732

733 5.4. Application of our Mg/Ca-temperature regression

734 Our species-specific equations were applied to convert Mg/Ca into temperature (Figure 7).
 735 While our regional Mg/Ca to temperature relations were established on the basis of only
 736 samples for which we have δ¹⁸O measurements and thereby direct estimates of foraminiferal
 737 calcification depths at the respective core site, we applied the equations to all samples where
 738 we measured Mg/Ca ratios (see. Table 1). Temperatures obtained from *G. ruber* and *G.*
 739 *elongatus* match mixed layer temperatures. Mg/Ca temperatures of *G. sacculifer* correspond to
 740 temperatures from the mixed layer bottom and uppermost thermocline. Mg/Ca temperatures
 741 calculated from *P. obliquiloculata* and *N. dutertrei* reflect upper and those calculated from *G.*
 742 *tumida* lower thermocline conditions. *P. obliquiloculata* and *N. dutertrei* are most suitable to

743 track changes in NPTW and SPTW since they calcify at water depths corresponding to the core
744 of these water masses.

745



746

747 **Figure 7.** (a) Mg/Ca temperatures calculated by applying the newly established species-
748 specific calibrations projected on CTD temperature profiles (grey lines). Horizontal bars denote
749 temperature errors, calculated following the method described in *Mohtadi et al.* [2014].
750 Colored vertical bars indicate calcification depth ranges resulting from the application of our
751 species-specific Mg/Ca-temperature calibrations. (b) For comparison, we show shell $\delta^{18}\text{O}$ -
752 derived calcification depth estimates for all species in combination. Gray lines indicate depth
753 profiles of predicted $\delta^{18}\text{O}_c$ calculated from CTD casts. Samples where only Mg/Ca or $\delta^{18}\text{O}$
754 measurements are available are marked with stars.

755

756 6. Conclusions

757 We presented novel, paired Mg/Ca and $\delta^{18}\text{O}$ measurements on multispecies planktic
758 foraminifera tests from accurately dated modern surface sediments in combination with water
759 column data (CTD and $\delta^{18}\text{O}_{\text{SW}}$) from the WPWP. Based on CTD salinity and $\delta^{18}\text{O}_{\text{SW}}$ we
760 establish new $\delta^{18}\text{O}_{\text{SW}}$ -salinity regressions for surface (mixed layer) and subsurface
761 (thermocline) waters (NPTW and SPTW) in the WPWP. Our data imply that it is reasonable
762 to apply different $\delta^{18}\text{O}_{\text{SW}}$ -salinity regressions for surface and thermocline water masses. Due

763 to very similar regression lines for the Philippines and PNG areas, individual regressions for
764 sub(surface) waters from both areas can be combined into more robust equations representing
765 the entire study area. These equations are $\delta^{18}\text{O}_{\text{sw}} = 0.37 \cdot \text{S} - 12.4$ for surface and $\delta^{18}\text{O}_{\text{sw}} =$
766 $0.33 \cdot \text{S} - 11.0$ for thermocline waters.

767

768 Shell $\delta^{18}\text{O}$ -derived estimates reveal that the calcification depths of planktic foraminifera
769 offshore the Philippines and offshore PNG are very similar. Our estimates match results from
770 other areas, and reveal that, also in the WPWP, *G. ruber* and *G. elongatus* reflect mixed layer
771 conditions (0-80 m), *G. sacculifer* reflects bottom of mixed layer and uppermost thermocline
772 conditions (45-85 m). *P. obliquiloculata* and *N. dutertrei* preserve upper (90-160 m) and *G.*
773 *tumida* lower thermocline conditions (230-265 m). Hence, our data imply that these species are
774 the best choice to reconstruct thermocline conditions in the WPWP. *N. dutertrei* inhabits a
775 slightly larger depth range than *P. obliquiloculata* in the WPWP. Therefore, *P. obliquiloculata*
776 might be more suitable to reconstruct the upper thermocline. Previous thermocline
777 reconstructions that are based on other species need to be reconsidered in face of the new
778 results. For example, shell $\delta^{18}\text{O}$ does not indicate different habitat depths for *G. ruber* and *G.*
779 *elongatus*. Hence, for the WPWP, the data do not support the use of *G. ruber* – *G. elongatus*
780 records to reconstruct variations in the vertical structure of the upper water column.

781

782 Our newly established regional multispecies Mg/Ca-temperature regression is within the range
783 of published multispecies and species-specific Mg/Ca-temperature calibrations ($\text{Mg}/\text{Ca} = 0.26$
784 $\exp 0.097 \cdot \text{T}$ as calculated using reduced major axis regression). However, the Mg/Ca
785 temperature relation of most individual species is more accurately described by species-specific
786 calibrations. We find that the regional regressions for *G. ruber*, *G. elongatus* and *G. tumida* are
787 similar to the species-specific or multispecies equations published by *Dekens et al.* [2002] and
788 *Anand et al.* [2003]. Calcification temperatures of *G. sacculifer*, *P. obliquiloculata* and *N.*
789 *dutertrei* are exceptionally warm in the western tropical Pacific and thus, require regional,
790 species-specific calibrations. The application of previously published calibrations would
791 underestimate the calcification temperatures of these species. Using a reduced major axis
792 regression we calculate the species-specific calibration $\text{Mg}/\text{Ca} = 0.24 \exp 0.097 \cdot \text{T}$ for *G.*
793 *sacculifer* and $\text{Mg}/\text{Ca} = 0.21 \exp 0.097 \cdot \text{T}$ for *P. obliquiloculata* and *N. dutertrei*. Nevertheless,
794 further studies are needed to confirm the applicability of these calibrations for the open Pacific
795 Ocean and for paleo-reconstructions.

797 **Acknowledgments**

798 We would like to thank the captains, crews, and the scientific shipboard parties of expeditions
 799 SO–228 and RR–1313. We thank Henning Kuhnert, Birgit Meyer-Schack and Ryan Bu for
 800 technical assistance. John Southon (UC Irvine) is acknowledged for performing radiocarbon
 801 measurements. GeoB sample material was stored, curated and supplied by the GeoB Core
 802 Repository at the MARUM – Center for Marine Environmental Sciences, University of
 803 Bremen, Germany. RR samples were provided by the Rutgers Core Repository. We thank two
 804 anonymous reviewers for their constructive comments, which helped to improve the quality of
 805 our manuscript. The work is funded by the DFG-Research Center / Cluster of Excellence “The
 806 Ocean in the Earth System”, the BMBF project 03G0228A (EISPAC) and by the NSF project
 807 OCE1131371. The data reported in this paper will be made available on Pangaea
 808 (www.pangaea.de) and WDS (www.icsu-wds.org).

809

810 **References**

- 811 Allen, K. A., B. Hönisch, S. M. Eggins, L. L. Haynes, Y. Rosenthal, and J. Yu (2016), Trace element proxies for
 812 surface ocean conditions: A synthesis of culture calibrations with planktic foraminifera, *Geochimica et*
 813 *Cosmochimica Acta*, 193, 197-221, doi:10.1016/j.gca.2016.08.015.
- 814 Anand, P., H. Elderfield, and M. H. Conte (2003), Calibration of Mg/Ca thermometry in planktonic foraminifera
 815 from a sediment trap time series, *Paleoceanography*, 18(2), 1050, doi:10.1029/2002PA000846.
- 816 Andreasen, D. J., and A. C. Ravelo (1997), Tropical Pacific Ocean thermocline depth reconstructions for the
 817 Last Glacial Maximum, *Paleoceanography*, 12(3), 395-413, doi:10.1029/97PA00822.
- 818 Arbuszewski, J., P. deMenocal, A. Kaplan, and E. C. Farmer (2010), On the fidelity of shell-derived
 819 $\delta^{18}\text{O}$ seawater estimates, *Earth and Planetary Science Letters*, 300(3-4), 185-196,
 820 doi:10.1016/j.epsl.2010.10.035.
- 821 Aurahs, R., Y. Treis, K. Darling, and M. Kucera (2011), A revised taxonomic and phylogenetic concept for the
 822 planktonic foraminifer species *Globigerinoides ruber* based on molecular and morphometric evidence, *Marine*
 823 *Micropaleontology*, 79(1-2), 1-14, doi:10.1016/j.marmicro.2010.12.001.
- 824 Barker, S., M. Greaves, and H. Elderfield (2003), A study of cleaning procedures used for foraminiferal Mg/Ca
 825 paleothermometry, *Geochem Geophys Geosy*, 4(9), 8407, doi:10.1029/2003GC000559.
- 826 Beaufort, L., T. de Garidel-Thoron, A. C. Mix, and N. G. Pisias (2001), ENSO-like forcing on oceanic primary
 827 production during the Late Pleistocene, *Science*, 293(5539), 2440-2444, doi:10.1126/science.293.5539.2440.
- 828 Bemis, B. E., H. J. Spero, J. Bijma, and D. W. Lea (1998), Reevaluation of the oxygen isotopic composition of
 829 planktonic foraminifera: Experimental results and revised paleotemperature equations, *Paleoceanography*,
 830 13(2), 150-160, doi:10.1029/98pa00070.
- 831 Berger, W. H., M. C. Bonneau, and F. L. Parker (1982), Foraminifera on the deep-sea floor: lysocline and
 832 dissolution rate, *Oceanologica Acta*, 5, 249-258.
- 833 Böhm, F., M. M. Joachimski, H. Lehnert, G. Morgenroth, W. Kretschmer, J. Vacelet, and W.-C. Dullo (1996),
 834 Carbon isotope records from extant Caribbean and South Pacific sponges: Evolution of $\delta^{13}\text{C}$ in surface water
 835 DIC, *Earth and Planetary Science Letters*, 139(1), 291-303, doi:10.1016/0012-821X(96)00006-4.
- 836 Bolliet, T., A. Holbourn, W. Kuhnt, C. Laj, C. Kissel, L. Beaufort, M. Kienast, N. Andersen, and D. Garbe-
 837 Schonberg (2011), Mindanao Dome variability over the last 160 kyr: Episodic glacial cooling of the West
 838 Pacific Warm Pool, *Paleoceanography*, 26(1), PA1208, doi:10.1029/2010pa001966.
- 839 Bouvier-Soumagnac, Y., and J. C. Duplessy (1985), Carbon and oxygen isotopic composition of planktonic
 840 foraminifera from laboratory culture, plankton tows and Recent sediment: implications for the reconstruction of
 841 paleoclimatic conditions and of the global carbon cycle, *Journal of Foraminiferal Research*, 15, 302-320.

842 Boyle, E. A., and L. D. Keigwin (1985), Comparison of Atlantic and Pacific paleochemical records for the last
843 215,000 years: changes in deep ocean circulation and chemical inventories, *Earth and Planetary Science*
844 *Letters*, 76, 135-150.

845 Cléroux, C., E. Cortijo, P. Anand, L. Labeyrie, F. Bassinot, N. Caillon, and J.-C. Duplessy (2008), Mg/Ca and
846 Sr/Ca ratios in planktonic foraminifera: Proxies for upper water column temperature reconstruction,
847 *Paleoceanography*, 23(3), PA3214, doi:10.1029/2007pa001505.

848 Craig, H., and L. I. Gordon (1965), Deuterium and oxygen-18 variations in the ocean and the marine
849 atmosphere, in *Stable isotope in oceanographic studies and paleotemperatures*, edited by E. Tongiorgi, pp. 9-
850 130, Spoleto, Pisa (Consiglio Nazionale delle Ricerche, Laboratorio di Geologia Nucleare).

851 de Garidel-Thoron, T., Y. Rosenthal, L. Beaufort, E. Bard, C. Sonzogni, and A. C. Mix (2007), A multiproxy
852 assessment of the western equatorial Pacific hydrography during the last 30 kyr, *Paleoceanography*, 22,
853 PA3204, doi:10.1029/2006PA001269.

854 Dekens, P. S., D. W. Lea, D. K. Pak, and H. J. Spero (2002), Core top calibration of Mg/Ca in tropical
855 foraminifera: Refining paleotemperature estimation, *Geochemistry, Geophysics, Geosystems*, 3(4), 1022,
856 doi:10.1029/2001GC000200.

857 DiNezio, P. N., A. Clement, G. A. Vecchi, B. Soden, A. J. Broccoli, B. L. Otto-Bliesner, and P. Braconnot
858 (2011), The response of the Walker circulation to Last Glacial Maximum forcing: Implications for detection in
859 proxies, *Paleoceanography*, 26(3), PA3217, doi:10.1029/2010PA002083.

860 Elderfield, H., and G. Ganssen (2000), Past temperature and $\delta^{18}\text{O}$ of surface ocean waters inferred from
861 foraminiferal Mg/Ca ratios, *Nature*, 405(6785), 442-445, doi:10.1038/35013033.

862 Epstein, S., and T. Mayeda (1953), Variation of O^{18} content of waters from natural sources, *Geochimica et*
863 *Cosmochimica Acta*, 4, 213-224.

864 Evans, D., B. S. Wade, M. Henehan, J. Erez, and W. Müller (2016), Revisiting carbonate chemistry controls on
865 planktic foraminifera Mg / Ca: implications for sea surface temperature and hydrology shifts over the
866 Paleocene–Eocene Thermal Maximum and Eocene–Oligocene transition, *Climate of the Past*, 12(4), 819-835,
867 doi:10.5194/cp-12-819-2016.

868 Fairbanks, R. G. (1982), The origin of Continental Shelf and Slope Water in the New York Bight of Maine:
869 Evidence from $\text{H}_2^{18}\text{O}/\text{H}_2^{16}\text{O}$ Ratio Measurements, *Journal of Geophysical Research*, 87(C8), 5796-5808.

870 Fairbanks, R. G., C. D. Charles, and J. D. Wright (1992), Origin of global meltwater pulses, in *Radiocarbon*
871 *after four decades*, edited by R. E. Taylor, pp. 473-500, Springer Verlag.

872 Fairbanks, R. G., M. N. Evans, J. L. Rubenstone, R. A. Mortlock, K. Broad, M. D. Moore, and C. D. Charles
873 (1997), Evaluating climate indices and their geochemical proxies measured in corals, *Coral Reefs*, 16, 93-100.

874 Farmer, E. C., A. Kaplan, P. B. de Menocal, and J. Lynch-Stieglitz (2007), Corroborating ecological depth
875 preferences of planktonic foraminifera in the tropical Atlantic with the stable oxygen isotope ratios of core top
876 specimens, *Paleoceanography*, 22(3), doi:10.1029/2006PA001361.

877 Ferguson, J. E., G. M. Henderson, M. Kucera, and R. E. M. Rickaby (2008), Systematic change of foraminiferal
878 Mg/Ca ratios across a strong salinity gradient, *Earth and Planetary Science Letters*, 265(1-2), 153-166,
879 doi:10.1016/j.epsl.2007.10.011.

880 Fine, R. A., R. Lukas, F. M. Bingham, M. J. Warner, and R. H. Gammon (1994), The western equatorial Pacific
881 - a water mass crossroads, *Journal of Geophysical Research*, 99(C12), 25063-25080, doi:10.1029/94jc02277.

882 Friedli, H., H. Löttscher, H. Oeschger, U. Siegenthaler, and B. Stauffer (1986), Ice core record of the $^{13}\text{C}/^{12}\text{C}$
883 ratio of atmospheric CO_2 in the past two centuries, *Nature*, 324, 237-238.

884 Gagan, M. K., E. J. Hendy, S. G. Haberle, and W. S. Hantoro (2004), Post-glacial evolution of the Indo-Pacific
885 Warm Pool and El Niño–Southern oscillation, *Quaternary International*, 118-119, 127-143, doi:10.1016/s1040-
886 6182(03)00134-4.

887 Gordon, A. L. (1986), Inter-ocean exchange of thermocline water, *Journal of Geophysical Research*, 91(C4),
888 5037, doi:10.1029/JC091iC04p05037.

889 Hertzberg, J. E., and M. W. Schmidt (2013), Refining *Globigerinoides ruber* Mg/Ca paleothermometry in the
890 Atlantic Ocean, *Earth and Planetary Science Letters*, 383, 123-133, doi:10.1016/j.epsl.2013.09.044.

891 Higgins, H. W., D. J. Mackey, and L. Clementson (2006), Phytoplankton distribution in the Bismarck Sea north
892 of Papua New Guinea: The effect of the Sepik River outflow, *Deep-Sea Research Part I: Oceanographic*
893 *Research Papers*, 53(11), 1845-1863, doi:10.1016/j.dsr.2006.09.001.

894 Hönisch, B., K. A. Allen, D. W. Lea, H. J. Spero, S. M. Eggins, J. Arbuszewski, P. deMenocal, Y. Rosenthal, A.
895 D. Russell, and H. Elderfield (2013), The influence of salinity on Mg/Ca in planktic foraminifera – Evidence
896 from cultures, core-top sediments and complementary $\delta^{18}\text{O}$, *Geochimica et Cosmochimica Acta*, 121, 196-213,
897 doi:10.1016/j.gca.2013.07.028.

898 Hut, G. (1987), Consultants group meeting on stable isotopic reference samples for geochemical and
899 hydrological investigations, edited, p. 42, International Atomic Energy Agency, Vienna.

900 Isobe, T., E. D. Feigelson, M. G. Akritas, and G. J. Babu (1990), Linear Regression in Astronomy I., *The*
901 *Astrophysical Journal*, 364, 104-113.

902 Kawahata, H. (2005), Stable isotopic composition of two morphotypes of *Globigerinoides ruber* (white) in the
903 subtropical gyre in the North Pacific, *Paleontological Research*, 9(1), 27-35.

904 Kawahata, H., A. Nishimura, and M. K. Gagan (2002), Seasonal change in foraminiferal production in the
905 western equatorial Pacific warm pool: evidence from sediment trap experiments, *Deep-Sea Research Part II:
906 Topical Studies in Oceanography*, 49(13-14), 2783-2800, doi:10.1016/S0967-0645(02)00058-9.

907 Kim, S.-T., and J. R. O'Neil (1997), Equilibrium and nonequilibrium oxygen isotope effects in synthetic
908 carbonates, *Geochim Cosmochim Acta*, 61(16), 3461-3475, 10.1016/s0016-7037(97)00169-5.

909 Kısakürek, B., A. Eisenhauer, F. Böhm, D. Garbe-Schönberg, and J. Erez (2008), Controls on shell Mg/Ca and
910 Sr/Ca in cultured planktonic foraminifera, *Globigerinoides ruber* (white), *Earth and Planetary Science Letters*,
911 273(3-4), 260-269, doi:10.1016/j.epsl.2008.06.026.

912 Kuroyanagi, A., and H. Kawahata (2004), Vertical distribution of living planktonic foraminifera in the seas
913 around Japan, *Marine Micropaleontology*, 53(1-2), 173-196, DOI 10.1016/j.marmicro.2004.06.001.

914 Lea, D. W., T. A. Mashiotta, and H. J. Spero (1999), Controls on magnesium and strontium uptake in planktonic
915 foraminifera determined by live culturing, *Geochimica Et Cosmochimica Acta*, 63(16), 2369-2379,
916 doi:10.1016/S0016-7037(99)00197-0.

917 Lea, D. W., D. K. Pak, and H. J. Spero (2000), Climate impact of late quaternary equatorial Pacific sea surface
918 temperature variations, *Science*, 289(5485), 1719-1724.

919 Leech, P. J., J. Lynch-Stieglitz, and R. Zhang (2013), Western Pacific thermocline structure and the Pacific
920 marine Intertropical Convergence Zone during the Last Glacial Maximum, *Earth and Planetary Science Letters*,
921 363, 133-143, doi:10.1016/j.epsl.2012.12.026.

922 LeGrande, A. N., and G. A. Schmidt (2006), Global gridded data set of the oxygen isotopic composition in
923 seawater, *Geophysical Research Letters*, 33(12), doi:10.1029/2006gl026011.

924 LeGrande, A. N., and G. A. Schmidt (2011), Water isotopologues as a quantitative paleosalinity proxy,
925 *Paleoceanography*, 26(3), doi:10.1029/2010pa002043.

926 Locarnini, R. A., et al. (2013), *World Ocean Atlas 2013, Volume 1: Temperature.*, U.S. Government Printing
927 Office, Washington, D.C.

928 Lončarić, N., F. J. C. Peeters, D. Kroon, and G.-J. A. Brummer (2006), Oxygen isotope ecology of recent
929 planktic foraminifera at the central Walvis Ridge (SE Atlantic), *Paleoceanography*, 21(3),
930 doi:10.1029/2005pa001207.

931 Martin, P. A., and D. W. Lea (2002), A simple evaluation of cleaning procedures on fossil benthic foraminiferal
932 Mg/Ca, *Geochem Geophys Geosy*, 3(10), 1-8, doi:10.1029/2001gc000280.

933 Mathien-Blard, E., and F. Bassinot (2009), Salinity bias on the foraminifera Mg/Ca thermometry: Correction
934 procedure and implications for past ocean hydrographic reconstructions, *Geochemistry, Geophysics,
935 Geosystems*, 10(12), doi:10.1029/2008gc002353.

936 McConnell, M. C., and R. C. Thunell (2005), Calibration of the planktonic foraminiferal Mg/Ca
937 paleothermometer: Sediment trap results from the Guaymas Basin, Gulf of California, *Paleoceanography*,
938 20(2), doi:10.1029/2004pa001077.

939 Mohtadi, M., S. Steinke, J. Groeneveld, H. G. Fink, T. Rixen, D. Hebbeln, B. Donner, and B. Herunadi (2009),
940 Low-latitude control on seasonal and interannual changes in planktonic foraminiferal flux and shell
941 geochemistry off south Java: A sediment trap study, *Paleoceanography*, 24(1), PA1201,
942 doi:10.1029/2008pa001636.

943 Mohtadi, M., D. W. Oppo, A. Luckge, R. DePol-Holz, S. Steinke, J. Groeneveld, N. Hemme, and D. Hebbeln
944 (2011), Reconstructing the thermal structure of the upper ocean: Insights from planktic foraminifera shell
945 chemistry and alkenones in modern sediments of the tropical eastern Indian Ocean, *Paleoceanography*, 26(3),
946 PA3219, doi:10.1029/2011pa002132.

947 Mohtadi, M., M. Prange, D. W. Oppo, R. De Pol-Holz, U. Merkel, X. Zhang, S. Steinke, and A. Luckge (2014),
948 North Atlantic forcing of tropical Indian Ocean climate, *Nature*, 509(7498), 76-80, doi:10.1038/nature13196.

949 Mohtadi, M., et al. (2013), Report and preliminary results of RV SONNE cruise SO-228, Kaohsiung-
950 Townsville, 04.05.2013- 23.06.2013, EISPAC-WESTWIND-SIODP. Berichte aus dem MARUM und dem
951 Fachbereich Geowissenschaften der Universität Bremen, 295, 110 pp. urn:nbn:de:gbv:46-00103343-13.

952 Morimoto, M. (2002), Salinity records for the 1997-98 El Niño from Western Pacific corals, *Geophysical
953 Research Letters*, 29(11), doi:10.1029/2001gl013521.

954 Mulitza, S., D. Boltovskoy, B. Donner, H. Meggers, A. Paul, and G. Wefer (2003), Temperature: $\delta^{18}\text{O}$
955 relationships of planktonic foraminifera collected from surface waters, *Palaeogeography, Palaeoclimatology,
956 Palaeoecology*, 202(1-2), 143-152, doi:10.1016/s0031-0182(03)00633-3.

957 Niebler, H.-S., H.-W. Hubberten, and G. Gersonde (1999), Oxygen isotope values of planktic foraminifera: a
958 tool for the reconstruction of surface water stratification, in *Use of Proxies in Paleoceanography: Examples
959 from the South Atlantic*, edited by G. Fischer and G. Wefer, pp. 165-189, Springer-Verlag, Berlin, Heidelberg.
960 Nürnberg, D., J. Bijma, and C. Hemleben (1996), Assessing the reliability of magnesium in foraminiferal calcite
961 as a proxy for water mass temperatures, *Geochimica et Cosmochimica Acta*, 60(5), 803-814.

962 Nürnberg, D., A. Müller, and R. R. Schneider (2000), Paleo-sea surface temperature calculations in the
963 equatorial east Atlantic from Mg/Ca ratios in planktic foraminifera: A comparison to sea surface temperature
964 estimates from Uk37, oxygen isotopes, and foraminiferal transfer function, *Paleoceanography*, 15(1), 124-134,
965 10.1029/1999PA000370.

966 Patrick, A., and R. C. Thunell (1997), Tropical Pacific sea surface temperatures and upper water column thermal
967 structure during the Last Glacial Maximum, *Paleoceanography*, 12(5), 649-657, doi:10.1029/97pa01553.

968 Peeters, F. J. C., G.-J. A. Brummer, and G. Ganssen (2002), The effect of upwelling on the distribution and
969 stable isotope composition of *Globigerina bulloides* and *Globigerinoides ruber* (planktic foraminifera) in
970 modern surface waters of the NW Arabian Sea, *Global and Planetary Change*, 34(3-4), 269-291,
971 doi:10.1016/S0921-8181(02)00120-0.

972 Radenac, M.-H., and M. Rodier (1996), Nitrate and chlorophyll distributions in relation to thermohaline and
973 current structures in the western tropical Pacific during 1985-1989, *Deep Sea Research Part II: Topical Studies*
974 *in Oceanography*, 4-6, 725-752.

975 Radenac, M. H., F. Leger, M. Messie, P. Dutrieux, C. Menkes, and G. Eldin (2016), Wind-driven changes of
976 surface current, temperature, and chlorophyll observed by satellites north of New Guinea, *J Geophys Res-*
977 *Oceans*, 121(4), 2231-2252, 10.1002/2015JC011438.

978 Ravelo, A. C., and C. Hillaire-Marcel (2007), Chapter Eighteen The Use of Oxygen and Carbon Isotopes of
979 Foraminifera in Paleoclimatology, 1, 735-764, doi:10.1016/s1572-5480(07)01023-8.

980 Regenberg, M., S. Steph, D. Nürnberg, R. Tiedemann, and D. Garbe-Schönberg (2009), Calibrating Mg/Ca
981 ratios of multiple planktonic foraminiferal species with $\delta^{18}\text{O}$ -calcification temperatures: Paleothermometry for
982 the upper water column, *Earth and Planetary Science Letters*, 278(3-4), 324-336,
983 doi:10.1016/j.epsl.2008.12.019.

984 Regoli, F., T. de Garidel-Thoron, K. Tachikawa, Z. Jian, L. Ye, A. W. Droxler, G. Lenoir, M. Crucifix, N.
985 Barbarin, and L. Beaufort (2015), Progressive shoaling of the equatorial Pacific thermocline over the last eight
986 glacial periods, *Paleoceanography*, 30(5), 439-455, doi:10.1002/2014pa002696.

987 Rickaby, R. E. M., and P. Halloran (2005), Cool La Niña During the Warmth of the Pliocene?, *Science*,
988 307(5717), 1948-1952, doi:10.1126/science.1104666.

989 Rippert, N., D. Nürnberg, J. Raddatz, E. Maier, E. Hathorne, J. Bijma, and R. Tiedemann (2016), Constraining
990 foraminiferal calcification depths in the western Pacific warm pool, *Marine Micropaleontology*, 128, 14-27,
991 doi:10.1016/j.marmicro.2016.08.004.

992 Rosenthal, Y., and G. P. Lohmann (2002), Accurate estimation of sea surface temperatures using dissolution-
993 corrected calibrations for Mg/Ca paleothermometry, *Paleoceanography*, 17(3), 16-11-16-16, 1044,
994 10.1029/2001pa000749.

995 Rosenthal, Y., E. A. Boyle, and N. Slowey (1997), Temperature control on the incorporation of magnesium,
996 strontium, fluorine, and cadmium into benthic foraminiferal shells from Little Bahama Bank: Prospects for
997 thermocline paleoceanography, *Geochimica Et Cosmochimica Acta*, 61(17), 3633-3643, doi:10.1016/S0016-
998 7037(97)00181-6.

999 Rosenthal, Y., M. P. Field, and R. M. Sherrell (1999), Precise determination of element/calcium ratios in
1000 calcareous samples using sector field inductively coupled plasma mass spectrometry, *Analytical Chemistry*,
1001 71(15), 3248-3253, doi:10.1021/AC981410x.

1002 Rosenthal, Y., et al. (2004), Interlaboratory comparison study of Mg/Ca and Sr/Ca measurements in planktonic
1003 foraminifera for paleoceanographic research, *Geochem Geophys Geosy*, 5, doi:10.1029/2003GC000650.

1004 Russell, A. D., B. Hönisch, H. J. Spero, and D. W. Lea (2004), Effects of seawater carbonate ion concentration
1005 and temperature on shell U, Mg, and Sr in cultured planktonic foraminifera, *Geochimica et Cosmochimica Acta*,
1006 68(21), 4347-4361, 10.1016/j.gca.2004.03.013.

1007 Sagawa, T., Y. Yokoyama, M. Ikehara, and M. Kuwae (2012), Shoaling of the western equatorial Pacific
1008 thermocline during the last glacial maximum inferred from multispecies temperature reconstruction of
1009 planktonic foraminifera, *Palaeogeography, Palaeoclimatology, Palaeoecology*, 346-347, 120-129,
1010 doi:10.1016/j.palaeo.2012.06.002.

1011 Schlitzer, R. (2014), Ocean Data View, odv.awi.de, edited.

1012 Shackleton, N. (1974), Attainment of isotopic equilibrium between ocean water and the benthonic foraminifera
1013 genus *Uvigerina*: Isotopic changes in the ocean during the last glacial, in *Les méthodes quantitatives d'étude des*
1014 *variations du climat au cours du Pléistocène*, edited by L. Labeyrie, pp. 203-209, CNRS, Paris.

1015 Spero, H. J., K. M. Mielke, E. M. Kalve, D. W. Lea, and D. K. Pak (2003), Multispecies approach to
1016 reconstructing eastern equatorial Pacific thermocline hydrography during the past 360 kyr, *Paleoceanography*,
1017 18(1), doi:10.1029/2002PA000814.

1018 Spero, H. J., S. M. Eggins, A. D. Russell, L. Vetter, M. R. Kilburn, and B. Hönisch (2015), Timing and
1019 mechanism for intratest Mg/Ca variability in a living planktic foraminifer, *Earth and Planetary Science Letters*,
1020 409, 32-42, 10.1016/j.epsl.2014.10.030.

1021 Steinke, S., H.-Y. Chiu, P.-S. Yu, C.-C. Shen, L. Löwemark, H.-S. Mii, and M.-T. Chen (2005), Mg/Ca ratios of
1022 two *Globigerinoides ruber* (white) morphotypes: Implications for reconstructing past tropical/subtropical
1023 surface water conditions, *Geochemistry, Geophysics, Geosystems*, 6(11), doi:10.1029/2005gc000926.
1024 Steph, S., M. Regenberg, R. Tiedemann, S. Mulitza, and D. Nürnberg (2009), Stable isotopes of planktonic
1025 foraminifera from tropical Atlantic/Caribbean core-tops: Implications for reconstructing upper ocean
1026 stratification, *Marine Micropaleontology*, 71(1-2), 1-19, doi:10.1016/j.marmicro.2008.12.004.
1027 Tachikawa, K., A. Timmermann, L. Vidal, C. Sonzogni, and O. E. Timm (2014), CO₂ radiative forcing and
1028 Intertropical Convergence Zone influences on western Pacific warm pool climate over the past 400 ka,
1029 *Quaternary Science Reviews*, 86(0), 24-34, doi:10.1016/j.quascirev.2013.12.018.
1030 Thirumalai, K., J. N. Richey, T. M. Quinn, and R. Z. Poore (2014), *Globigerinoides ruber* morphotypes in the
1031 Gulf of Mexico: a test of null hypothesis, *Scientific reports*, 4, 6018, doi:10.1038/srep06018.
1032 Thunell, R., E. Tappa, C. Pride, and E. Kincaid (1999), Sea-surface temperature anomalies associated with the
1033 1997/1998 El Niño recorded in the oxygen isotope composition of planktonic foraminifera, *Geology*, 27(9), 843-
1034 846.
1035 Tsuchiya, M., R. Lukas, and R. Fine (1989), Source Waters of the Pacific Equatorial Undercurrent, *Progress in*
1036 *Oceanography*, 23, 46.
1037 van Geldern, R., and J. A. C. Barth (2012), Optimization of instrument setup and post-run corrections for
1038 oxygen and hydrogen stable isotope measurements of water by isotope ratio infrared spectroscopy (IRIS),
1039 *Limnology and Oceanography: Methods*, 10(12), 1024-1036, doi:10.4319/lom.2012.10.1024.
1040 Vecchi, G. A., B. J. Soden, A. T. Wittenberg, I. M. Held, A. Leetmaa, and M. J. Harrison (2006), Weakening of
1041 tropical Pacific atmospheric circulation due to anthropogenic forcing, *Nature*, 441(7089), 73-76,
1042 doi:10.1038/nature04744.
1043 Wang, L. J. (2000), Isotopic signals in two morphotypes of *Globigerinoides ruber* (white) from the South China
1044 Sea: implications for monsoon climate change during the last glacial cycle, *Palaeogeogr Palaeocl*, 161(3-4),
1045 381-394, doi:10.1016/S0031-0182(00)00094-8.
1046 Watkins, J. M., A. C. Mix, and J. Wilson (1996), Living planktic foraminifera: Tracers of circulation and
1047 productivity regimes in the central equatorial Pacific, *Deep Sea Research Part II: Topical Studies in*
1048 *Oceanography*, 43(4-6), 26.
1049 Xu, J. A., W. Kuhnt, A. Holbourn, M. Regenberg, and N. Andersen (2010), Indo-Pacific Warm Pool variability
1050 during the Holocene and Last Glacial Maximum, *Paleoceanography*, 25(4), PA4230,
1051 doi:10.1029/2010PA001934.
1052 Yamasaki, M., A. Sasaki, M. Oda, and H. Domitsu (2008), Western equatorial Pacific planktic foraminiferal
1053 fluxes and assemblages during a La Niña year (1999), *Marine Micropaleontology*, 66(3-4), 304-319,
1054 doi:10.1016/j.marmicro.2007.10.006.
1055 Zenk, W., G. Siedler, A. Ishida, J. Holfort, Y. Kashino, Y. Kuroda, T. Miyama, and T. J. Müller (2005),
1056 Pathways and variability of the Antarctic Intermediate Water in the western equatorial Pacific Ocean, *Progress*
1057 *in Oceanography*, 67, 245-281, doi:10.1016/j.pocean.2005.05.003.
1058 Zweng, M. M., et al. (2013), *World Ocean Atlas 2013, Volume 2: Salinity*, Washington, D.C.
1059

1060

1061